Medizinische Fakultät

der

Universität Duisburg-Essen

Aus der Klinik für Neurologie

Mesenchymal stromal cell-derived small extracellular vesicles induce ischemic neuroprotection by modulating leukocytes and specifically polymorphonuclear neutrophils

Inauguraldissertation

zur

Erlangung des Doktorgrades der Medizin

durch die Medizinische Fakultät

der Universität Duisburg-Essen

Vorgelegt von

Chen Wang

aus China

2020

DOI: 10.17185/duepublico/73649
URN: urn:nbn:de:hbz:464-20210204-072944-6

Dekan: Herr Univ.-Prof. Dr. med. J. Buer

1. Gutachter/in: Herr Univ.-Prof. Dr. med. D. M. Hermann

2. Gutachter/in: Herr Prof. Dr. rer. nat. B. Giebel

3. Gutachter/in: Herr Prof. Dr. med. J. Minnerup

Tag der mündlichen Prüfung: 02. Dezember 2020

List of publications

de Carvalho, T.S., Sanchez-Mendoza, E.H., Schultz Moreira, A.R., Nascentes Melo, L.M., **Wang, C.**, Sardari, M., Hagemann, N., Doeppner, T.R., Kleinschnitz, C., and Hermann, D.M. (2020). Hypocaloric Diet Initiated Post-Ischemia Provides Long-Term Neuroprotection and Promotes Peri-Infarct Brain Remodeling by Regulating Metabolic and Survival-Promoting Proteins. Mol Neurobiol. https://doi.org/10.1007/s12035-020-02207-7

Sardari, M., Skuljec, J., Yin, D., Zec, K., de Carvalho, T.S., Albers, D., **Wang, C.**, Pul, R., Popa-Wagner, A., Doeppner, T.R., Kleinschnitz, C., Dzyubenko, E., and Hermann, D.M. (2020). Lipopolysaccharide-induced sepsis-like state compromises post-ischemic neurological recovery, brain tissue survival and remodeling via mechanisms involving microvascular thrombosis and brain T cell infiltration. Brain Behav Immun. https://doi.org/10.1016/j.bbi.2020.10.015

Wang, C., Börger, V., Sardari, M., Murke F., Skuliec, J., Pul, R., Hagemann, N., Dzyubenko, E., Dittrich R., Gregorius, J., Hasenberg M., Kleinschnitz, C., Popa-Wagner, A., Doeppner, T., Gunzer, M., Giebel, B., Hermann, D. (2020). Mesenchymal Stromal Cell-Derived Small Extracellular Vesicles Induce Ischemic Neuroprotection by Modulating Leukocytes and Specifically Neutrophils. Stroke 51, 1825-1834.

Contents

1. INTRODUCTION

1.1. Pathophysiology of acute ischemic stroke

1.1.1. Ischemic stroke and therapy

As far back as 400 BC, the ancient Greek physician Hippocrates first described the phenomenon of sudden limb paralysis, which is known today as stroke (Poirier and Derouesné, 1993). Stroke can be caused either by interruption of the blood flow to the brain (ischemic stroke) or by the rupture of a blood vessel of the brain (hemorrhagic stroke). Ischemic stroke occurs in approximately 87% of all stroke patients (Benjamin et al., 2019). In 2016, the global prevalence of ischemic stroke was 67.6 million and a total of 2.7 million individuals died of this disease (Benjamin et al., 2019). To date, these numbers are still increasing, which makes ischemic stroke one of leading causes of death worldwide (Benjamin et al., 2019).

Ischemic stroke is the most prevalent cause of long-term disability, which imposes economic burden on the society (Benjamin et al., 2019; Taylor et al., 1996). Yet, the therapeutic options are limited to thrombolysis and thrombectomy. Recombinant tissue plasminogen activator (rtPA) has hitherto been the only thrombotic agent approved by U.S. Food and Drug Administration (FDA) for the treatment of ischemic stroke since 1996 (National Institute of Neurological Disorders and Stroke rt-PA Stroke Study Group, 1995). However, several disadvantages severely limit its clinical application: the narrow applicable time window up to 4.5 hours post symptom onset, the contraindications before thrombolysis application, and the potential adverse effect of serious bleeding after thrombolysis (Wardlaw et al., 2014). Therefore, only a small proportion of stroke patients benefit from rtPA. Recently, endovascular thrombectomy has been emerging as an alternative and add-on treatment to systemic thrombolysis. Despite numerous advances, such as a larger therapeutic window up to as wide as 12 hours after stroke onset and a

better efficacy in the recanalization of large vessel occlusions, many crucial challenges remain, including its practical implementation and cost effectiveness (Evans et al., 2017). Researchers have been investigating and translating experimental knowledge from bench to bedside. Unfortunately, neuroprotectants that initially appeared promising in cell culture and animal models have repeatedly failed in clinical trials (Drummond et al., 2000; Xu and Pan, 2013). The failures can be the result of multiple factors. Undoubtedly, a better understanding of the immune mechanisms in the pathophysiology of ischemic stroke may open promising avenues for the development of novel stroke therapeutics.

1.1.2. Role of polymorphonuclear neutrophils (PMNs) in acute ischemic stroke

Inflammation and immunity are key elements of the pathophysiology of ischemic stroke (Iadecola and Anrather, 2011). The innate immune system plays a critical role in post-ischemic neuroinflammation. In the brain, this immune response comprises the activation of brain-resident microglia and recruitment of blood-derived leukocytes (Chamorro et al., 2012). In the acute phase of the inflammatory response, dying and dead cells release "danger signals", namely danger-associated molecular patterns (DAMPs), to activate pattern recognition receptors (PRRs), such as Toll-like receptors (TLRs), which are widely expressed on microglia and brain endothelial cells, resulting in the expression of proinflammatory mediators that promote the infiltration of leukocytes (Chamorro et al., 2012; Iadecola and Anrather, 2011). Subsequently, brain-invading immune cells further induce the secondary brain injury by releasing reactive oxygen species (ROS), proteases, and cytokines/chemokines, causing blood-brain barrier disruption, brain edema, hemorrhagic transformation, and neuronal death (Jickling et al., 2015).

Polymorphonuclear neutrophils (PMNs), the most abundant type of leukocytes and an essential component of the innate immune system, play a decisive role in brain injury and neurological recovery poststroke (Hermann and Gunzer, 2019). PMNs already appear in brain parenchyma at 12 hours and peak within 24-72 hours after ischemic stroke

(Garcia et al., 1994; Gelderblom et al., 2009). The cerebral accumulation of PMNs is associated with the severity of brain damage and poor neurological outcome both in humans (Akopov et al., 1996; Maestrini et al., 2015) and in rodents (Herz et al., 2015; Matsuo et al., 1994). In peripheral blood, high neutrophil-lymphocyte ratios were found to predict poor neurological recovery, which further supports that PMNs play a detrimental role in ischemic injury and brain remodeling (Hermann and Gunzer, 2019; Hermann et al., 2018; Xue et al., 2017). Indeed, depletion of PMNs by anti-Ly6G antibody or prevention of PMN brain entry by C-X-C motif chemokine receptor 2 (CXCR2) or very-late-antigen-4 (VLA-4) blockade has been shown to reduce neurological deficits and infarct volume in numerous preclinical studies (Hermann and Gunzer, 2019; Herz et al., 2015; Neumann et al., 2015). However, strategies that prevent PMN brain entry after stroke have not been translated successfully into the clinical setting (Veltkamp and Gill, 2016). In the phase II study ACTION (Safety and efficacy of natalizumab in patients with acute ischemic stroke), Natalizumab, a humanized monoclonal antibody against VLA-4, did not influence infarct growth (Elkins et al., 2017). In a phase III clinical trial, Enlimomab, a murine monoclonal antibody against intercellular adhesion molecule 1 (ICAM-1), failed to show benefits and even increased mortality in patients with acute ischemic stroke (Enlimomab Acute Stroke Trial Investigators, 2001). Despite these failures, novel therapeutic interventions targeting PMNs have been under investigation. Recently, mesenchymal stromal cells (MSCs) have been shown to exert potent immunomodulatory effects on PMNs such as the suppression of PMN activity and reduction of PMN infiltration, making MSCs a promising cell therapy for ischemic stroke (Joel et al., 2019).

1.2. Mesenchymal stromal cell (MSC)-derived therapies for ischemic stroke

1.2.1. MSCs for ischemic stroke therapy

MSCs were first discovered in the bone marrow of guinea pigs in the 1960s (Friedenstein et al., 1970). They are multipotent stromal cells that can differentiate into various cell types, including osteoblasts, chondroblasts, and adipocytes (Ankrum et al., 2014). MSCs can also differentiate into cerebral parenchymal cells such as neurons and astrocytes in experimental animals (Kopen et al., 1999; Sanchez-Ramos et al., 2000). MSCs have great potential as therapeutic agents because (a) they are easy to harvest from a variety of tissues, including bone marrow, adipose tissue, and umbilical cord, (b) they have low immunogenicity due to the fact that MSCs do not express (or express only at very low levels) human leukocyte antigen (HLA) class II encoded antigens, and (c) they have potent immunomodulatory capabilities of regulating a broad range of immune cells, including PMNs, monocytes/macrophages, natural killer cells, T cells, and B cells (Börger et al., 2017; Joel et al., 2019; Klingemann et al., 2008; Shi et al., 2018).

Over the past two decades, preclinical studies investigating the effects of MSC treatment in ischemic stroke have demonstrated that MSC administration exerts neuroprotective and neurorestorative effects (Doeppner et al., 2015; Sarmah et al., 2018). The mechanism underlying the therapeutic action of MSCs was initially thought to be cell replacement. Engrafted MSCs were hypothesized to migrate to the ischemic brain tissue, to proliferate in the injured region, and finally to differentiate into brain cells. However, preclinical studies have shown that the MSC engraftment rate in damaged tissues is very low after intravenous administration, and that the low rate of differentiation of MSCs into parenchymal brain cells hardly contributes to functional improvement (Chen et al., 2001; Li et al., 2002). Recent evidence implies that MSCs mediate their therapeutic functions in a paracrine manner, and it has been suggested that these paracrine effects of MSCs might be mediated by MSC-derived small extracellular vesicles (MSC-sEVs) (Börger et

al., 2017; Doeppner et al., 2015; Gnecchi et al., 2016).

1.2.2. MSC-derived small extracellular vesicles (MSC-sEVs) for ischemic stroke therapy

Extracellular vesicles (EVs), which are released by virtually all cell types, are typically classified as exosomes, microvesicles, and apoptotic bodies according to their biogenesis. Exosomes are derived from multivesicular bodies (MVBs) fused with the plasma membrane. The size of exosomes typically varies between 60-150 nm. Microvesicles are formed and released by budding from the cell plasma membrane, resulting in vesicles with a size of 100-1,000 nm in diameter. Apoptotic bodies are released by apoptotic cells and have a broad size range of 50-2,000 nm in diameter (Börger et al., 2017; El Andaloussi et al., 2013; Tkach and Théry, 2016). Due to the lack of specific makers that identify their cellular origin, the generic term 'EVs' is used to refer to all experimentally-obtained vesicles, and it has been proposed that therapeutic activities of EVs mainly attribute to small EVs (sEVs) with a size of 60-150 nm resembling exosomes (Börger et al., 2017; Tkach and Théry, 2016; Vagner et al., 2019).

These sEVs have important functions in intercellular communication through the transfer of molecular cargos such as proteins and nucleic acids, and have emerged as a novel therapeutic strategy in human diseases (Shah et al., 2018). MSC-sEVs have previously been shown to promote neurological recovery and brain remodeling after focal cerebral ischemia (Doeppner et al., 2015; Xin et al., 2017a; Xin et al., 2013a; Zhang et al., 2019). In a mouse model of ischemic stroke, Doeppner et al. have demonstrated that MSC-sEV preparations, which were intravenously administered 24 hours after intraluminal middle cerebral artery occlusion (MCAO), were equally effective as their parental MSCs in alleviating motor-coordination deficits, in promoting long-term neuronal survival, angiogenesis, and neurogenesis, and in reversing post-ischemic lymphopenia in peripheral blood (Doeppner et al., 2015).

sEV-based therapies have various advantages over cell therapies: sEVs are not self-replicating and lack endogenous tumor formation potentials. Due to their small size, sEV products hardly cause microvascular occlusions and can be sterilized by filtration. Manufacture and delivery of sEVs is also easier than that of cells (Lener et al., 2015).

Despite many merits in MSC-sEV-based therapies, increasing evidence indicates that both MSCs and MSC-sEVs exhibit considerable donor-to-donor and intra-population heterogeneity that influences their therapeutic efficacy (Ferguson and Nguyen, 2016; Kim et al., 2019; Phinney, 2012; Willis et al., 2017). Since MSC-sEVs can hardly sense environmental conditions, their biological activity can be predicted more precisely than that of MSCs. Characterization of this heterogeneity and identification of the right cell sources are essential to produce therapeutically active MSC-sEVs for clinical application.

1.2.3. Hypoxia preconditioning as a modifier of the therapeutic efficacy of MSCs or MSC-sEVs

To maximize the therapeutic activity of MSC-sEVs, preconditioning strategies have been developed, including exposure to hypoxic stimuli, growth factors, cytokines or lipopolysaccharide (LPS), and genetical engineering (Baldari et al., 2017; Schafer et al., 2016). Xin et al. have shown that tailored MSC-sEVs enriched with miR-133b or miR-17−92 cluster induce amplified neuroplasticity and functional recovery in a rat model of ischemic stroke (Xin et al., 2017a; Xin et al., 2013b; Xin et al., 2017b). Unlike genetically engineered MSC-sEVs overexpressing one single specific molecular cargo, sEVs harvested from MSCs in response to preconditioning stimuli exhibit complex changes of cargos that can result in more pronounced effects.

Hypoxia is one of the most widely used approaches to modify functional and molecular properties of MSCs or/and MSC-sEVs. Hypoxia itself has pro-angiogenic effects, enhancing the self-renewing and proliferation capacity of MSCs presumably by regulating hypoxia-related miRNA expression (Mohd Ali et al., 2016; Saad et al., 2016).

sEVs secreted from MSCs grown in hypoxic conditions carry a panel of cargos that, compared with normoxia-conditioned MSC-sEVs, reduce myocardial injury after cardiac ischemia (Zhu et al., 2018a; Zhu et al., 2018b), improve renal recovery after acute kidney injury (Collino et al., 2019), enhance angiogenesis (Xue et al., 2018), promote neovascularization and graft survival (Han et al., 2018), promote bone fracture healing (Liu et al., 2019), and reduce cognitive impairment in a mouse model of Alzheimer disease (Cui et al., 2018). However, whether sEVs obtained from hypoxic MSCs are superior to sEVs from normoxic MSCs with respect to their neuroprotective efficacy remains unclear.

2. AIM OF THE STUDY

MSC-sEVs appear to be a promising novel stroke therapy, but several issues need to be addressed before their clinical application. In this study, we aimed (1) to evaluate MSC-sEV hereogeneity; (2) to compare the therapeutic efficacy of sEVs derived from hypoxia-preconditioned MSCs and sEVs from normoxic MSCs; and (3) to investigate the role of brain-invading leukocytes, specifically of PMNs, in MSC-sEV-induced neuroprotection. To this end, male C57Bl6/j mice were exposed to 30 minutes intraluminal MCAO followed by 24 hours or 72 hours reperfusion. After reperfusion onset, vehicle or sEVs prepared from conditioned media of MSCs raised from bone marrow samples of three randomly selected healthy human donors (sources 16.3, 31.2 and 41.5) were intravenously administered. sEVs obtained from MSCs (donor source 41.5) cultured under normoxic (21% O_2) and hypoxic (1% O_2) conditions were applied using the same protocol. PMNs were depleted by anti-Ly6G antibody (Clone 1A8) injection 24 hours before and 24 hours after MCAO in vehicle and MSC-sEV treated mice. Neurological deficits, ischemic injury, blood-brain barrier (BBB) integrity, peripheral blood distribution, and brain immune cell infiltration were evaluated over 24 hours and 72 hours.

3. MATERIALS AND METHODS

3.1. Legal issues, animal housing, randomization and blinding

Experiments were performed with local government approval (Bezirksregierung Düsseldorf) in accordance to EU guidelines (Directive 2010/63/EU) for the care and use of laboratory animals and ARRIVE guidelines. Experiments were strictly randomized. The experimenter performing the animal experiments and histochemical studies was fully blinded at all stages of the study by another researcher preparing the vehicle and MSC-derived small extracellular vesicle (MSC-sEV) solutions. These solutions received dummy names (solution A, B, C, D), which were unblinded after termination of the study. Animals were kept in a regular inverse 12h:12h light/dark cycle in groups of 5 animals/cage. Behavioral tests and animal surgeries were always performed in the morning hours throughout the study.

3.2. Statistical planning

Statistical planning was done by a sample size calculator (https://www.dssresearch.com/KnowledgeCenter/toolkitcalculators/samplesizecalculators.aspx). For behavioral tests, infarct volume and histochemical analyses, we initially postulated that MSC-sEVs modified the mean by 25%, which with an expected standard deviation of 30% of the mean required a sample size of 18 animals/group, given that the alpha error was 5% and the beta error (1–statistical power) was 20%. In the course of this study, we realized that effect size was larger. We therefore reduced the group size to 16 animals/ group and later to 5-8 animals/ group. Whenever a single or up to two animals were missing due to animal dropouts (**Table 3**, see page 24), we did not fill them up. Wherever more animals were lost, animals were complemented.

3.3. Isolation and characterization of MSCs and MSC-sEVs

3.3.1. Expansion and characterization of MSCs

Human MSCs were raised from bone marrow samples of healthy donors after informed consent according to the Declaration of Helsinki, as described previously (Kordelas et al., 2014). Obtained MSC were expanded in low glucose Dulbecco's modified Eagle medium (DMEM; Cat# 12-604F; Lonza, Cologne, Germany) supplemented with 10% human platelet lysate (hPL), 100 U/ ml penicillin-streptomycin-L-glutamine (Cat# 10378016; Thermo Fisher Scientific, Waltham, USA) and 5 IU/ml heparin (Heparin-Natrium-25000, Ratiopharm, Ulm, Germany) and passaged at approximately 80% confluency. In passage two, MSCs were characterized according to International Society of Cell and Gene Therapy (ISCT) standards (Dominici et al., 2006), as previously described (Kordelas et al., 2014; Radtke et al., 2016). Briefly, MSCs were stained with fluorochrome labeled anti-CD73, anti-CD90, anti-CD105, anti-CD31, anti-CD34 and anti-CD45 antibodies (**Table 5**, see page 32-33) and analysed on a multicolor flow cytometer (Cytoflex, Software Cytexpert 2.3; Beckman-Coulter, Krefeld, Germany). In addition, the osteogenic and adipogenic differentiation potentials of MSCs were confirmed in conventional MSC differentiation assays. Starting at passage 3, MSC conditioned media were harvested every 48 hours, centrifuged at 2,000 g for 15 minutes to remove cell debris and stored at -20°C until usage. Only conditioned media were used which lacked any mycoplasma contamination. (This part is done by our collaborator AG Giebel at the Institute for Transfusion Medicine, University Hospital Essen.)

3.3.2. Isolation of MSC-sEVs

MSC-sEVs were harvested from MSC-conditioned media exactly as described previously (Ludwig et al., 2018). Briefly, conditioned media were simultaneously thawed and

processed. To remove debris and larger vesicles, combined supernatants were centrifuged at 10,000 g for 45 minutes in an Avanti centrifuge (JA-10 rotor; k factor: 3610; Beckman-Coulter, Krefeld, Germany). Next, sEVs were concentrated by polyethylene glycol 6000 (PEG) precipitation. Finally, sEVs were washed in 0.9% NaCl and re-precipitated by ultracentrifugation at 110,000 g for 130 minutes (Ti45 rotor, k-factor: 133). sEV samples were solved in 10 mM Hepes/ 0,9% NaCl (Thermo Fisher Scientific, Waltham, USA) ($4x10^7$ cell equivalents per mL) and stored at -80°C. (This part is done by our collaborator AG Giebel at the Institute for Transfusion Medicine, University Hospital Essen.)

3.3.3. Characterization of MSC-sEV preparations by nanoparticle tracking analysis and Western blots

According to the recently updated ISEV guidelines (Théry et al., 2018), sEV fractions were characterized for concentration and size by nanoparticle tracking analysis (NTA; Particle Metrix, Meerbusch, Germany), as described previously (Kordelas et al., 2014; Sokolova et al., 2011). The protein concentrations were determined by a standardized bicinchoninic acid (BCA) assay according the manufacturer's protocol (Pierce, Rockford, IL, USA). For western blot, MSC-sEVs (30 µg) were solubilized with Laemmli sample buffer containing dithiothreitol (DTT; AppliChem, Darmstadt, Germany) and separated on 1D sodium dodecyl sulfate-polyacrylamide gel electrophoresis (SDS-PAGE) gels before transfer to polyvinylidene fluoride (PVDF) membranes (Millipore, Darmstadt, Germany). Membranes were blocked in 0.1 M phosphate-buffered saline (PBS) containing 0.1% Tween-20 (PBS-T) or 0.1 M Tris-buffered saline (TBS) containing 0.1% Tween-20 (TBS-T) that was supplemented with 5% (w/v) skim milk powder (Sigma-Aldrich, Munich, Germany). Membranes were sequentially stained with anti-syntenin (clone EPR8102; Abcam, Cambridge, UK), anti-prohibitin (clone II-14-10; Thermo Fisher Scientific, Waltham, USA) and anti-calnexin (ab10286; Abcam, Cambridge, UK) antibodies or with anti-CD81 (clone JS-81; BD Biosciences, San Jose, CA, USA), anti-

CD9 (clone VJ1/20.3.1; kindly provided by Francisco Sánchez, Madrid, Spain) and anti-CD63 (H5C6; BioLegend, San Diego, CA, USA) antibodies. Anti-syntenin, anti-CD81, anti-CD9 and anti-CD63 antibodies were used as sEV markers, anti-prohibitin and anti-calnexin antibodies as contamination markers. Membranes were washed and counterstained with appropriate horseradish peroxidase-conjugated secondary antibodies (Dianova, Hamburg, Germany) that were detected by enhanced chemiluminescence labeling. With non-overlapping sizes, syntenin, prohibitin and calnexin were stained on one membrane and CD81, CD9 and CD63 on another membrane. (This part is done by our collaborator AG Giebel at the Institute for Transfusion Medicine, University Hospital Essen.)

3.3.4. Transmission electron microscopy of MSC-sEVs

sEV samples were diluted 100 times in MilliQ water. 7.5 µl of the sample solution were mixed with 1 µl aqueous contrasting solution containing 1% methyl cellulose (w/v; Sigma Aldrich) and 2% uranyl acetate (w/v; Polysciences, Warrington, FL, USA). After an incubation of 10 minutes, a 0.5 µl droplet was placed on a 200 mesh copper grid covered with a carbon coated formvar film (Plano, Wetzlar, Germany) and dried at room temperature to allow the MSC-sEVs to adhere to the film surface. Images were acquired using a JEM 1400Plus electron microscope (JEOL, Tokyo, Japan) operating at 120 kV that was equipped with a 4096x4096 pixel CMOS camera (TemCam-F416; TVIPS, Gauting, Germany). Image acquisition software EMMENU (Version 4.09.83) was used for taking 16 bit images. Image post-processing was carried out using the software ImageJ (Version 1.52b; National Institutes of Health, Bethesda, MD, USA). (This part is done by our collaborator AG Gunzer at the Institute of Experimental Immunology and Imaging, University Hospital Essen.)

3.4. Animal groups and MSC-sEV preparations used for evaluating post-ischemic neuroprotection

A total of 289 male C57BL6/J mice aged 8-10 weeks (Harlan Laboratories, Darmstadt, Germany) were studied in a total of seven sets of mice. In animal set I, mice were exposed to intraluminal MCAO and vehicle (n=16 animals) or sEVs harvested under regular conditions (21% O_2 in ambient air) from MSC source 16.3 (n=17 animals), MSC source 31.2 (n=18) or MSC source 41.5 (n=16) were intravenously administered immediately after reperfusion onset. In animal set II, mice were also submitted to MCAO and vehicle (n=16 animals) or sEVs collected from MSCs harvested under regular conditions (21% O_2; source 41.5; n=16; 'normoxic') or hypoxic conditions (1% O_2 in controlled hypoxia chamber; source 41.5; n=16) were intravenously applied after reperfusion onset. In animal sets III and IV, 200 µg control IgG (clone 2A3; BioXCell, West Lebanon, NH, U.S.A.) or anti-Ly6G antibody (clone 1A8; BioXCell) were intraperitoneally administered 24 hours before and 24 hours after MCAO as control treatment or for PMN depletion (Herz et al., 2015; Neumann et al., 2015). In set III, vehicle or sEVs collected under regular conditions (21% O_2; source 41.5) were intravenously applied and in set IV vehicle or sEVs collected under hypoxic conditions (1% O_2; source 41.5) were intravenously administered. Thus, these mice were assigned to four groups receiving control IgG/vehicle (n=14 animals), control IgG/sEVs harvested under regular conditions (21% O_2; n=15), anti-Ly6G/vehicle (n=15) and anti-Ly6G/sEVs harvested under regular conditions (21% O_2; n=15) (animal set III) and to four groups receiving control IgG/vehicle (n=7), control IgG/sEVs harvested under hypoxic conditions (1% O_2; n=7), anti-Ly6G/vehicle (n=5) and anti-Ly6G/sEVs harvested under hypoxic conditions (1% O_2; n=7) (animal set IV). In all four sets of mice, behavioral deficits were studied, and brain injury was evaluated by infarct volumetry and immunohistochemistry at 72 hours after MCAO. In animal sets V and VI, we again exposed mice to MCAO. Animal sets V and VI were treated as sets III and IV with control IgG/vehicle (n=7 and 8, respectively),

control IgG/sEVs harvested under regular conditions (21% O_2; source 41.5; n=8 and 9), anti-Ly6G/vehicle (n=8 each) and anti-Ly6G/sEVs harvested under regular conditions (21% O_2; source 41.5; n=8 and 9). In these mice brain immune infiltrates and peripheral blood leukocytes were studied by flow cytometry at 72 hours after MCAO. Set VII was exposed to sham-anesthesia and treated with vehicle (n=5) or sEVs harvested under regular conditions (21% O_2; source 41.5; n=5) or exposed to MCAO and treated with vehicle (n=7) or sEVs harvested under regular conditions (21% O_2; source 41.5; n=7). In these mice, peripheral blood leukocyte count and leukocyte activation were examined by flow cytometry at 24 hours after sham operation or MCAO, and ischemic injury and brain immune cell infiltration were examined by infarct volumetry and immunohistochemistry. Flow chart of animal experiments is described in **Table 3** (for table 3, see page 24).

To explore the heterogeneity of MSC-sEVs, we administered MSC-sEV preparations from three randomly selected human donors (sources 16.3, 31.2, and 41.5). For the preparation of animal set I, two independent sEV preparations of MSC source 16.3 and two independent sEV preparations of MSC source 41.5 were used (labeled (A) and (B)), which were injected into 9 and 8 animals (source 16.3) and 8 and 8 animals (source 41.5), respectively (**Table 1**). For MSC source 31.2, a single preparation was used throughout this study (labeled (A), administered to 18 animals) (**Table 1**). In animal set II, a single sEV preparation of source 41.5 (labeled (B), used for 16 animals) and two independent sEV preparations of source 41.5_{hypox} (labeled (A) and (B), used for 8 animals each) were applied (**Table 1**). The 41.5_{hypox} sEV preparation (B) was also administered to 10 animals in animal set IV and the 41.5 sEV preparation (B) to 12 animals in animal set VII (**Table 1**). In animal sets III, V, and VI, a single sEV preparation of source 41.5 (labeled (C)) was administered to 30, 16, and 18 animals, respectively (**Table 1**). All MSC-sEV preparations fulfilled state-of-the-art characteristics of sEVs according to the recently updated ISEV guidelines (Théry et al., 2018). They contained comparable amounts of particles and protein per ml final MSC-sEV preparation (**Table 1**).

Table 1: Characteristics of the MSC-sEV preparations used in this study including sets and animal numbers performed with each individual preparation.

MSC-sEV preparation	Animal set, in which preparation was used (number of animals)	Particle concentration [particles/ ml]	Particle size [nm]	Protein concentration [µg/ µl]	Purity [particles/ mg protein]
16.3 (A)	I (9)	$1.48x10^{11}$	132.5	3.38	$4.4x10^{10}$
16.3 (B)	I (8)	$5.80x10^{11}$	115.6	10.84	$5.3x10^{10}$
31.2 (A)	I (18)	$2.80x10^{11}$	108.2	7.70	$3.6x10^{10}$
41.5 (A)	I (8)	$1.48x10^{11}$	119.2	5.48	$2.7x10^{10}$
41.5 (B)	I (8) II (16) VII (12)	$1.16x10^{11}$	132.2	5.61	$2.1x10^{10}$
41.5 (C)	III (30) V (16) VI (18)	$1.60x10^{11}$	125.6	4.80	$3.3x10^{10}$
41.5_{hypox} (A)	II (8)	$8.4x10^{10}$	132.6	1.39	$6.0x10^{10}$
41.5_{hypox} (B)	II (8) IV (14)	$2.8x10^{11}$	119.7	2.41	$1.2x10^{11}$

In the left column, letters (A) – (C) refer to independent MSC-sEV preparations that were administered in the four animal sets defined in the second column.

3.5. Ischemic stroke model, animal exclusion criteria and dropouts

3.5.1. Intraluminal stroke model and MSC-sEV delivery

Surgical materials and equipment were listed in **Table 2** (see page 23) and focal cerebral ischemia was induced as shown in **Fig. 1**. Briefly, mice were anaesthetized with 1.0-1.5% isoflurane in a mixture of 30% O_2 and 70% N_2O. 200 µl Buprenorphine (0.1 mg/kg; Reckitt Benckiser, Slough, UK) was subcutaneously administered pre-operatively. Rectal temperature was maintained between 36.5 and 37.0°C using a feedback-controlled heating system. Cerebral blood flow was recorded by laser Doppler flowmetry (LDF) with a flexible probe attached to the skull above the core of left MCA territory for up to 15 minutes after reperfusion onset **(Fig. 1B)**. A midline neck incision was made; The left common carotid artery (CCA), external carotid artery (ECA) and internal carotid artery (ICA) were clearly isolated and exposed **(Fig. 1C)**. Once CCA and ECA were ligated, and ICA was temporarily clipped, a silicon-coated monofilament was inserted through a small incision on the CCA into the ICA to occlude the MCA **(Fig. 1D, 1E)**. Following 30 minutes of ischemia, the occluding filament was removed to induce reperfusion. Immediately thereafter, 200 µl normal saline (as vehicle) or $2x10^6$ cell equivalents of MSC-sEV preparations dissolved in 200 µl normal saline were administered through the animals' tail vein. Carprofen (4mg/kg; Norbrook, Newry, UK) was subcutaneously injected for post-operative pain relief during the first 3 days after surgery.

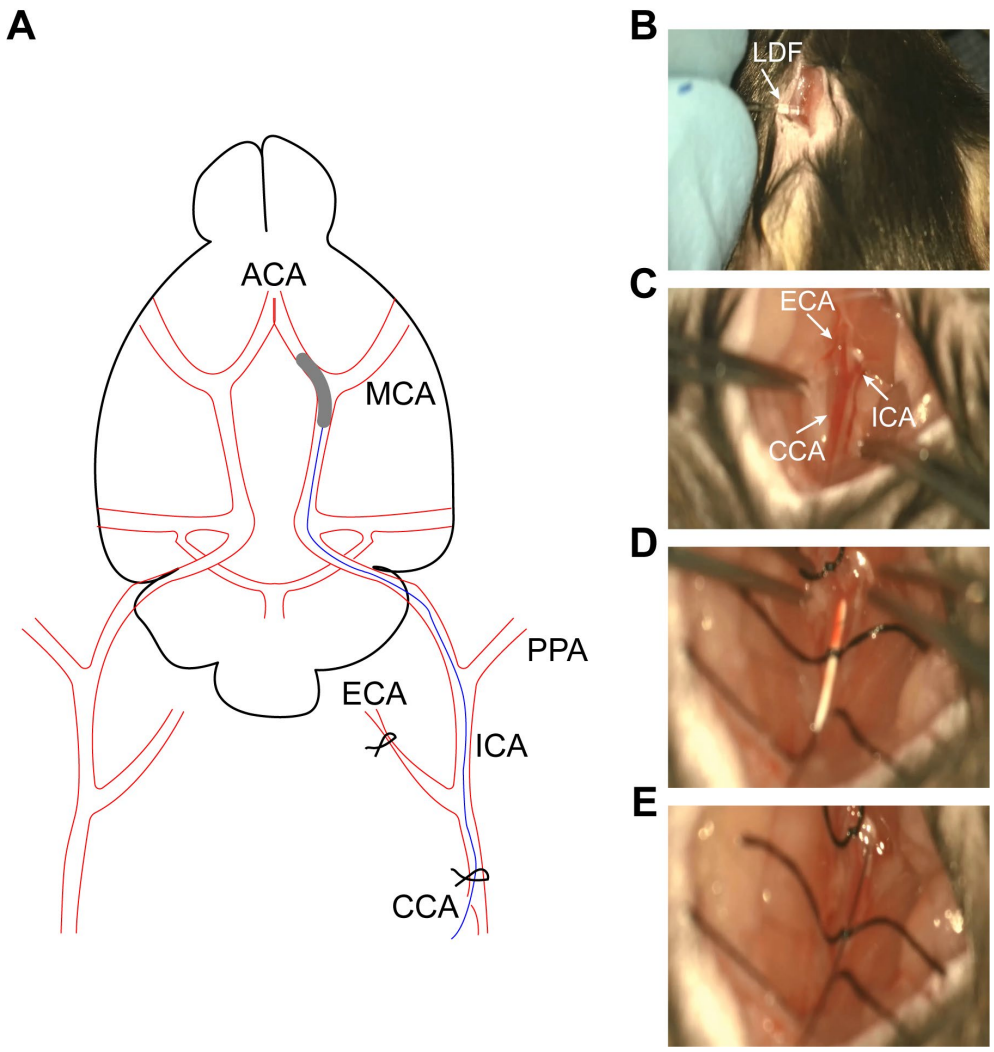

Figure 1. Scheme of ischemic stroke model. (A) Schematic diagram of intraluminal middle cerebral artery occlusion (MCAO). **(B)**, **(C)**, **(D)**, and **(E)** Representative pictures under the surgical microscope showing sequential steps of operation: **(B)** A laser Doppler flow (LDF) probe is attached to the skull overlying the middle cerebral artery (MCA) territory. **(C, D)** A silicon-coated monofilament is inserted into the cerebral vasculature via a small incision of the common carotid artery (CCA). **(E)** The monofilament is advanced across the skull base to occlude the MCA at its offspring. ACA, anterior carotid artery; ECA, external carotid artery; PPA, pterygopalatine artery; ICA, internal carotid artery.

Table 2. Surgical materials and equipment used for inducing focal cerebral ischemia.

Materials and equipment	Manufacturer
Carl Zeiss OPMI surgical microscope	Carl Zeiss, Oberkochen, Germany
Feedback-controlled heating system	Harvard apparatus, Holliston, USA
Halsey micro needle holder (Cat# 12500-12)	Fine Science Tools, Heidelberg, Germany
Laser Doppler flowmetry (LDF) system	Perimed Instruments, Rommerskirchen, Germany
Silicon-coated monofilament (Cat# 702234PK5Re)	Doccol, Sharon, MA, USA
Silk suture 5-0 (Cat# K890H), 7-0 (Cat# EH7464G)	Ethicon, Norderstedt, Germany
Spring scissors (Cat# 15024-10)	Fine Science Tools, Heidelberg, Germany
Standard scissors (Cat# 14568-12)	Fine Science Tools, Heidelberg, Germany
Vannas spring scissors (Cat# 15000-00)	Fine Science Tools, Heidelberg, Germany
Vascular clip, 9 mm long (Cat# FD562R)	Fisher Scientific, Schwerte, Germany

3.5.2. Animal exclusion criteria and dropouts

Mice were excluded from the study when they met one of the following exclusion criteria: (1) prolonged surgery duration >20 minutes; (2) drop of blood flow <75% after monofilament insertion; (3) lack of reperfusion after monofilament withdrawal; (4) >20% weight loss, respiratory abnormalities (central apneas) or death within 3 days after MCAO. A total of 22 mice were excluded. The detailed animal flow is summarized in **Table 3**.

Table 3: Flow chart of animal experiments.

Animal set	Group	Animals excluded				Animals enrolled
		(1)	(2)	(3)	(4)	
Set I	ischemic vehicle	–	–	1	1	16
	ischemic sEV 16.3	1	–	–	1	17
	ischemic sEV 31.2	–	–	–	1	18
	ischemic sEV 41.5	–	1	–	1	16
Set II	ischemic vehicle	–	–	1	1	16
	ischemic sEV 41.5	–	1	–	1	16
	ischemic sEV 41.5_{hypox}	–	–	–	1	16
Set III	ischemic isotype/ vehicle	–	–	–	2	14
	ischemic isotype/ sEV 41.5	–	–	–	1	15
	ischemic anti-Ly6G/ vehicle	–	1	–	–	15
	ischemic anti-Ly6G/ sEV 41.5	–	–	–	1	15
Set IV	ischemic isotype/ vehicle	–	–	–	–	7
	ischemic isotype/ sEV 41.5_{hypox}	–	–	–	–	7
	ischemic anti-Ly6G/ vehicle	–	–	–	–	5
	ischemic anti-Ly6G/ sEV 41.5_{hypox}	–	–	–	–	7
Set V	isotype/vehicle	–	–	1	1	7
	isotype/41.5 sEVs	–	–	–	1	8
	anti-Ly6G/vehicle	–	–	–	–	8
	anti-Ly6G/41.5 sEVs	–	–	–	–	8
Set VI	ischemic isotype/ vehicle	–	–	–	1	8
	ischemic isotype/ sEV 41.5	–	–	–	–	9
	ischemic anti-Ly6G/ vehicle	–	–	–	1	8
	ischemic anti-Ly6G/ sEV 41.5	–	–	–	–	9
Set VII	non-ischemic vehicle	–	–	–	–	5
	non-ischemic sEV 41.5	–	–	–	–	5
	ischemic vehicle	–	–	–	–	7
	ischemic sEV 41.5	–	–	–	–	7
Total		1	3	3	15	289

3.6. Analysis of neurological deficits

Neurological deficits were evaluated blindly at 1, 2 and 3 days post-MCAO using the modified Clark score (Clark et al., 1997) that contains a general and focal deficit scale, of which a total score ranging from 0 (healthy) to 39 (the worst performance) was calculated (**Table 4**).

Table 4. Modified Clark score.

General deficits (total score 0-13)	
1. Hair (score 0-2)	
Mouse observed on open bench top (OS). Observation with no interference.	
1.1. Hair neat and clean.	0
1.2. Lack of grooming, piloerection and dirt on the fur around nose and eyes.	1
1.3. Lack of grooming, piloerection and dirty coat, extending beyond just nose and eyes.	2
2. Eyes (score 0-4)	
Mouse on OS. Observation with no interference or stimulation.	
2.1. Open and clear (no discharge)	0
2.2. Open and characterized by milky white mucus.	1
2.3. Open and characterized by milky dark mucus.	2
2.4. Eyes clotted (one or both sides).	3
2.5. Closed.	4
3. Posture (score 0-4)	
Place the mouse on the palm of your hand and rock gently to observe stability.	
3.1. The mouse stands in the upright position on four limbs with the back parallel to the palm. During the rocking movement, it uses its limbs to stabilize itself.	0

3.2. The mouse stands humpbacked. During the rocking movement, it lowers its body instead of using its limbs to gain stability.	1
3.3. The head or part of the trunk lies on the palm.	2
3.4. The mouse reclines to one side but may be able to turn to an upright position with some difficulty.	3
3.5. No upright position possible.	4

4. Spontaneous activity (score 0-3; duration 1 minute)

Mouse on OS. Observation with no interference or stimulation.

4.1. The mouse is alert and explores actively.	0
4.2. The mouse seems alert, but it is calm and quiet and it starts and stops exploring repeatedly and slow.	1
4.3. The mouse is listless, moves sluggishly but does not explore.	2
4.4. The mouse is lethargic or stuporous and barely moves during the 1 minute.	3

Focal deficits (total score 0-26)

5. Body symmetry (score 0-2)

Mouse on OS, observation of undisturbed resting behavior and description of the virtual nose-tail line.

5.1. Normal. a, Body: normal posture, trunk elevated from the bench, with forelimbs and hindlimbs leaning beneath the body. b, Tail: straight	0
5.2. Slight asymmetry. a, Body: leans on one side with forelimbs and hindlimbs leaning beneath the body. b, Tail: slightly bent	1
5.3. Moderate asymmetry. a, Body: lean on one side with forelimbs and hindlimbs stretched out. b, Tail: slightly bent	2

6. Gait (score 0-4)

Mouse on OS. Observation of undisturbed movements.

6.1. Normal. Gait is flexible, symmetric, and quick.	0
6.2. Stiff, inflexible. The mouse walks humpbacked, slower than normal mouse.	1

6.3. Limping with asymmetric movements. 2

6.4. More severe limping, drifting, falling with obvious deficiency in gait. 3

6.5. Does not walk spontaneously. (In this case, stimulation will be performed gently pushing the mouse with a pen. When stimulated, the mouse walks no longer than three steps) 4

7. Climbing (score 0-3)

Mouse is placed in the center of a gripping surface at an angle of 45° to OS.

7.1. Normal. The mouse climbs quickly. 0

7.2. Climbs slowly, limb weakness present. 1

7.3. Holds onto slope, does not slip or climb. 2

7.4. Slides down slope, unsuccessful effort to prevent fall. 3

8. Circling behavior (score 0-3)

Mouse on OS. Observation of the mouse walking undisturbed on the OS.

8.1. Circling behavior absent. The mouse turns equally to left or right. 0

8.2. Predominantly one-sided turns. Optional: record to which side the mouse turns. 1

8.3. Circles to one side, although not constantly. 2

8.4. Circles constantly to one side. This one is now highlighted in yellow. 3

9. Forelimb symmetry (score 0-4)

Mouse suspended by the tail. Movements and position of forelimbs are observed.

9.1. Normal. Both forelimbs are extended towards the bench and move actively. 0

9.2. Light asymmetry. Contralateral forelimb does not extend entirely. 1

9.3. Marked asymmetry. Contralateral forelimb bends towards the trunk. The body slightly bends on the side ipsilateral to the stroke. 2

9.4. Prominent asymmetry. Contralateral forelimb adheres to the trunk. 3

9.5. Slight asymmetry, no body/limb movement. 4

10. Compulsory circling (score 0-3)

Forelimbs on bench, hindlimbs suspended by tail. This position reveals the presence of the contralateral limb palsy. In this handstand position, limb weakness is displayed by a circling behavior when the animal attempts forward motion.

10.1. Absent. Normal extension of both forelimbs.	0
10.2. Both forelimbs extended but begins to circle predominantly to one side.	1
10.3. Circles only to one side and may fall to one side.	2
10.4. Pivots to one side sluggishly and does not rotate in a full circle. Mouse will fall to one side.	3

11. Whisker response (score 0-4)

Mouse is placed on the bench. Using a pen, touch the whiskers and the tip of ears gently from behind, first on the lesioned side and then on the contralateral side.

11.1. Normal symmetrical response. The mouse turns the head towards the stimulated side and withdraws from the stimulus.	0
11.2. Light asymmetry. The mouse withdraws slowly when stimulated on the paretic side. Normal response on the side ipsilateral to the stroke.	1
11.3. Prominent asymmetry. No response when stimulated on the paretic side. Normal response on the side ipsilateral to the stroke.	2
11.4. Absent response on the paretic side, slow response when stimulated on the side ipsilateral to the stroke.	3
11.5. Absent response bilaterally.	4

12. Gripping test of the forepaws (score 0-3)

Mouse is held by the tail on the wire bar cage lid, so that the forepaws touch the grid.

12.1. Mouse grasps the grid firmly with forepaws and tries to place the hind paws also onto the grid by pulling the hind paws under the body.	0
12.2. Mouse accesses the grid but has less power. A slight pull breaks the grip of the forepaws.	1
12.3. Mouse cannot grip with the impaired forepaw.	2
12.4. Mouse cannot grip the grip.	3

3.7. Measurement of infarct volume

20-µm-thick coronal brain cryostat sections collected at 1 mm intervals across the forebrain were stained with cresyl violet (Cat# C5042; Sigma-Aldrich, Munich, Germany). In all sections, infarct area was determined using the indirect method that corrects for brain swelling by outlining intact tissue in both hemispheres using ImageJ software (National Institutes of Health, Bethesda, MD, USA). Infarct volume was determined by integrating infarct areas from all brain sections.

3.8. Immunohistochemical analysis of brain injury, immune infiltrates and blood-brain barrier permeability

3.8.1. Tissue processing and immunohistochemistry

Mice were transcardially perfused with saline and 4% paraformaldehyde (PFA; Cat# 8187151000; Millipore, Darmstadt, Germany). Brains were removed and post-fixed at 4°C in 4% PFA for 24 h, and then immersed sequentially in 15% and 30% sucrose (Cat# S9378; Sigma-Aldrich, Munich, Germany) at 4°C until they sank to the bottom. After removing excess liquid surround the tissue, samples were immersed in isopentane (-80°C; Cat# 143501; AppliChem, Darmstadt, Germany) chilled in dry ice for few seconds and then transferred into -80°C freezer for long-term storage. 20-µm-thick coronal cryosections from the rostrocaudal level of the bregma (i.e. +1.0 to 0 mm anterior to bregma) were obtained in Leica CM 1950 cryostat (Leica, Wetzlar, Germany) and used for following immunostaining.

Sections were rinsed three times for 5 minutes in 0.01 M PBS, except for IgG immunohistochemistry, and immersed in 0.01 M PBS containing 0.1% Triton X-100 (Cat# X100; Sigma-Aldrich, Munich, Germany) and 10% normal donkey serum (Cat# D9663; Sigma-Aldrich, Munich, Germany) for 30 minutes at room temperature. Sections

were incubated overnight at 4°C in monoclonal rabbit anti-NeuN (neuronal nuclear antigen; Cat# ab177487; Abcam, Cambridge, UK), monoclonal rat anti-CD45 (cluster of differentiation-45; Cat# 05-1416, Merck Millipore, Darmstadt, Germany), monoclonal rat anti-Ly6G (lymphocyte antigen 6 locus G; clone 1A8; Cat# 127602; Biolegend, San Diego, CA, USA), polyclonal goat anti-ICAM-1 (intercellular adhesion molecule-1; Cat# AF796; R&D, Minneapolis, MN, USA) or Alexa Fluor-594 conjugated polyclonal donkey anti-IgG (Cat# A21203; Thermo Fisher Scientific, Waltham, USA). After rinsing, sections were incubated for 1 hour at room temperature in biotinylated or Alexa Fluor-594 conjugated secondary antibody, as appropriate. In NeuN stainings, DNA-fragmented, that is, irreversibly injured cells were also detected by terminal deoxynucleotidyl transferase dUTP nick end labeling (TUNEL) using a kit (Cat# 11684795910; Roche Diagnostics, Mannheim, Germany) according to the manufacturer's protocol. For fluorescence immunohistochemistry, which was performed for NeuN, Ly6G and ICAM-1, nuclei were counterstained with Hoechst 33342 (Cat# B2261; Sigma-Aldrich, Munich, Germany). For 3,3'-diaminobenzidine (DAB) staining, which was used for CD45, endogenous peroxidase was blocked with 0.03% H_2O_2 for 10 minutes at room temperature (Cat# 31642; Sigma-Aldrich, Munich, Germany). Sections were then incubated in streptavidin peroxidase (Cat# ab64269; Abcam, Cambridge, UK), revealed by immersion in DAB using an appropriate kit (Cat# ab64261; Abcam, Cambridge, UK), and counterstained with hematoxylin (Cat# T865; Carl Roth, Karsruhe, Germany).

3.8.2. Imaging and analysis

Immunofluorescence stainings were evaluated using a Zeiss AxioOberver.Z1 inverted microscope (Carl Zeiss, Jena, Germany) and DAB stainings were evaluated using an Olympus BX51 microscope (Olympus, Tokyo, Japan). NeuN, TUNEL, NeuN/TUNEL and Ly6G stainings were analyzed by counting labeled cells in the entire ischemic striatum. CD45 staining was examined by counting labeled cells in three defined regions

of interest (ROI; each measuring 352.8 μm x 265.6 μm) in the most lateral part (i.e., core) of the ischemic striatum directly adjacent to the external capsule. For the cell numbers determined in the three ROI, mean values were formed. ICAM-1 and IgG stainings were assessed by intensity measurement across the whole striatum. In the latter analyses, background stainings were determined in the homologous contralateral non-ischemic striatum that were subtracted from values determined in the ipsilateral ischemic striatum.

3.9. Flow cytometry of peripheral blood and brain immune infiltrates

Single cell suspensions for flow cytometry analysis were obtained as previously described (Herz et al., 2015) with small modifications. One milliliter blood samples were taken from the animals' hearts. After erythrocyte cell lysis with lysis buffer (BD Biosciences, New Jersey, USA) followed by two washing steps with PBS, leukocytes were stained for 30 minutes at 4°C using antibody cocktails listed in **Table 5**. Following transcardial perfusion with ice-cold 0.1 M PBS, brains were removed and dissected into ischemic (left) and contralateral (right) hemisphere. Single cell suspensions were obtained by meshing the ischemic hemisphere through a 70-μm cell strainer (Life Sciences, New York, NY, USA) and continuously rinsing with 1% 4-(2-hydroxyethyl)-1-piperazineethanesulfonic acid (HEPES)-buffered Roswell Park Memorial Institute (RPMI)-1640 medium (Thermo Fisher Scientific, Waltham, USA). Samples were centrifuged at 400 g for 10 min at room temperature. After supernatant removal, pellets were resuspended in 37% Percoll (GE Healthcare, Uppsala, Sweden) in 0.01 M HCl/ PBS. Samples were centrifuged at 2,800 g for 20 min at room temperature. Myelin and Percoll were aspirated and cell pellets washed twice in 0.1 M PBS. Leukocytes were labeled for 30 min at 4°C with antibody cocktails listed in **Table 5**. Cell suspensions were analyzed using a BD FACS Aria III cell sorter (BD Biosciences, New Jersey, USA) and evaluated using FlowJo software V10 (Ashland, OR, USA). Leukocyte numbers were quantified on a Cytoflex flow cytometer (Beckman-Coulter). The gating strategy is shown in **Fig. 2**.

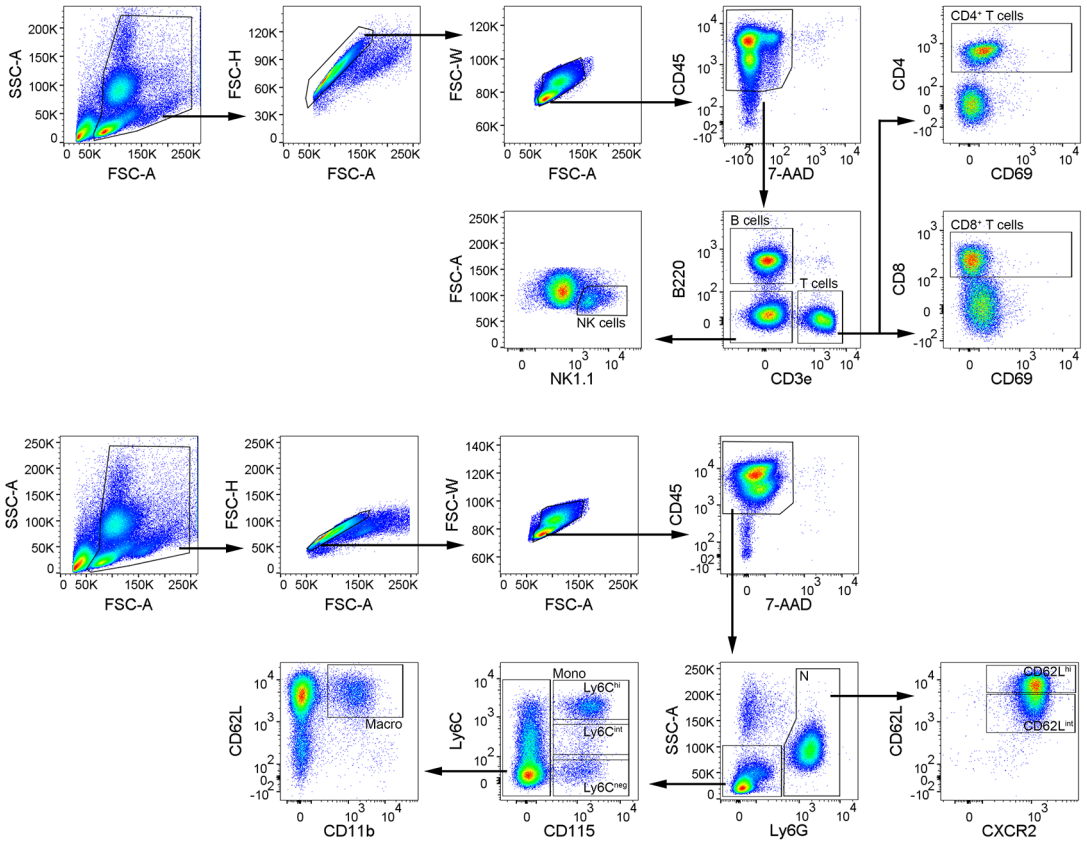

Figure 2. Gating strategy used for analyzing peripheral blood leukocytes and leukocyte activation via flow cytometry. Peripheral blood leukocytes were identified as CD45 expressing cells. Lineage antigens allowed their discrimination into lymphoid (upper gating strategy) and myeloid (lower gating strategy) subtypes. N, polymorphonuclear neutrophils; Mono, monocytes; Macro, macrophages.

Table 5. Antibodies used for flow cytometry.

Antigen	Conjugate	Host/isotype	Clone	Supplier
Mouse CD45	Pacific blue	Rat IgG2b, kappa	30F11	BioLegend
Mouse CD45	Brilliant violet (BV) 421	Rat IgG2b, kappa	30F11	BioLegend

Mouse CD45	BV 605	Rat IgG2b, kappa	30F11	BioLegend
Mouse Ly6G	Phycoerythrin (PE)	Rat IgG2a, kappa	1A8	BioLegend
Mouse CXCR2	Peridinin-chlorophyll (PerCP)-Cy5.5	Rat IgG2a, kappa	SA045E1	BioLegend
Mouse CD62L	eFluor 450	Rat IgG2a, kappa	MEL-14	eBioscience
Mouse Ly6C	PE-Cy7	Rat IgG2c, kappa	HK1.4	BioLegend
Mouse Ly6C	Fluorescein isothiocyanate (FITC)	Rat IgM, kappa	AL21	BD Biosciences
Mouse CD11b	Allophycocyanin (APC)	Rat IgG2b, kappa	M1/70	eBioscience
Mouse CD11b	PerCP-Cy5.5	Rat IgG2b, kappa	M1/70	BioLegend
Mouse CD115	PE-Cy7	Rat IgG2a, kappa	AFS98	eBioscience
Mouse CD3ε	Alexa Fluor 647	Hamster IgG	145-2C11	BioLegend
Mouse CD3	BV 510	Rat IgG2b, kappa	17A2	BioLegend
Mouse CD4	BV 605	Rat IgG2a, kappa	RM4-5	BD Biosciences
Mouse CD8	BV 786	Rat IgG2a, kappa	53-6.7	BD Biosciences
Mouse B220	PE	Rat IgG2a, kappa	RA3-6B2	BD Biosciences
Mouse CD19	APC	Rat IgG2a, kappa	1D3	BioLegend
Mouse NK-1.1	FITC	Rat IgG2a, kappa	PK136	BD Biosciences
Mouse CD69	PE-Cy7	Hamster IgG	H1.2F3	BioLegend
Human CD73	FITC	Mouse IgG_1, kappa	AD2	BD Biosciences
Human CD90	BV 605	Mouse IgG_1, kappa	5E10	BioLegend
Human CD105	BV 421	Mouse IgG_1, kappa	43A3	BioLegend
Human CD31	PE	Mouse IgG_1	1F11	Beckman-Coulter
Human CD34	APC 750	Mouse IgG_1	581	Beckman-Coulter
Human CD45	BV 785	Mouse IgG_1, kappa	HI30	BioLegend

3.10. Statistical analysis

Data were analysed by one-way analysis of variance (ANOVA) or repeated measurement ANOVA followed by least significant differences (LSD) tests (comparisons between ≥3 groups in normally distributed data), Kruskal-Wallis tests (comparisons between ≥3 groups in non-normally distributed data) or two-tailed t-tests (comparisons between 2 groups) as posthoc tests. Data were presented as mean ± standard deviation (SD) (longitudinal comparisons within the same animals) or box blots with median/ mean ± interquartile range (IQR) with minimum and maximum data as whiskers (all other comparisons between animals or tissue samples). SPSS 22.0 software (IBM, Armonk, NY, USA) was used for statistical analysis. P values <0.05 were considered significant.

4. RESULTS

4.1. Characterization of MSCs and MSC-sEVs

MSCs raised from healthy donors' bone marrow samples express MSC specific cell surface antigens, including CD73, CD90, and CD105, and lack expression of endothelial and hematopoietic marker proteins, including CD31, CD34, and CD45 (**Fig. 3A**). In addition, they have a typical fibroblastoid morphology with osteogenic and adipogenic differentiation potentials (**Fig. 3B**).

All MSC-sEV preparations used within this study have typical morphology and size (**Fig. 4**). They contain the exosomal marker proteins syntenin, CD81, CD9, and CD63. In contrast to prohibitin and calnexin, markers for cytosolic contamination, which are expressed in the cell lysate control but not in any of the sEV preparations (**Fig. 5**).

Legend to Figure 3 (for figure see page 36). Cells raised from bone marrow samples of healthy donors fulfill *bona fide* mesenchymal stromal cell (MSC) characteristics. **(A)** MSC surface antigens (CD73, CD90, and CD105), and endothelial and hematopoietic marker proteins as negative controls (CD31, CD34, and CD45) were assessed by flow cytometry. **(B)** MSC morphology (phase contrast image in left column), osteogenic differentiation potential (calcium aggregates in alizarin red stainings in mid column) and adipogenic differentiation potential (lipid vacuoles in oil red o stainings in right column) were assessed by conventional assays. Inserts in the mid and right column indicate negative controls. (Data are produced by our collaborator AG Giebel at the Institute for Transfusion Medicine, University Hospital Essen.)

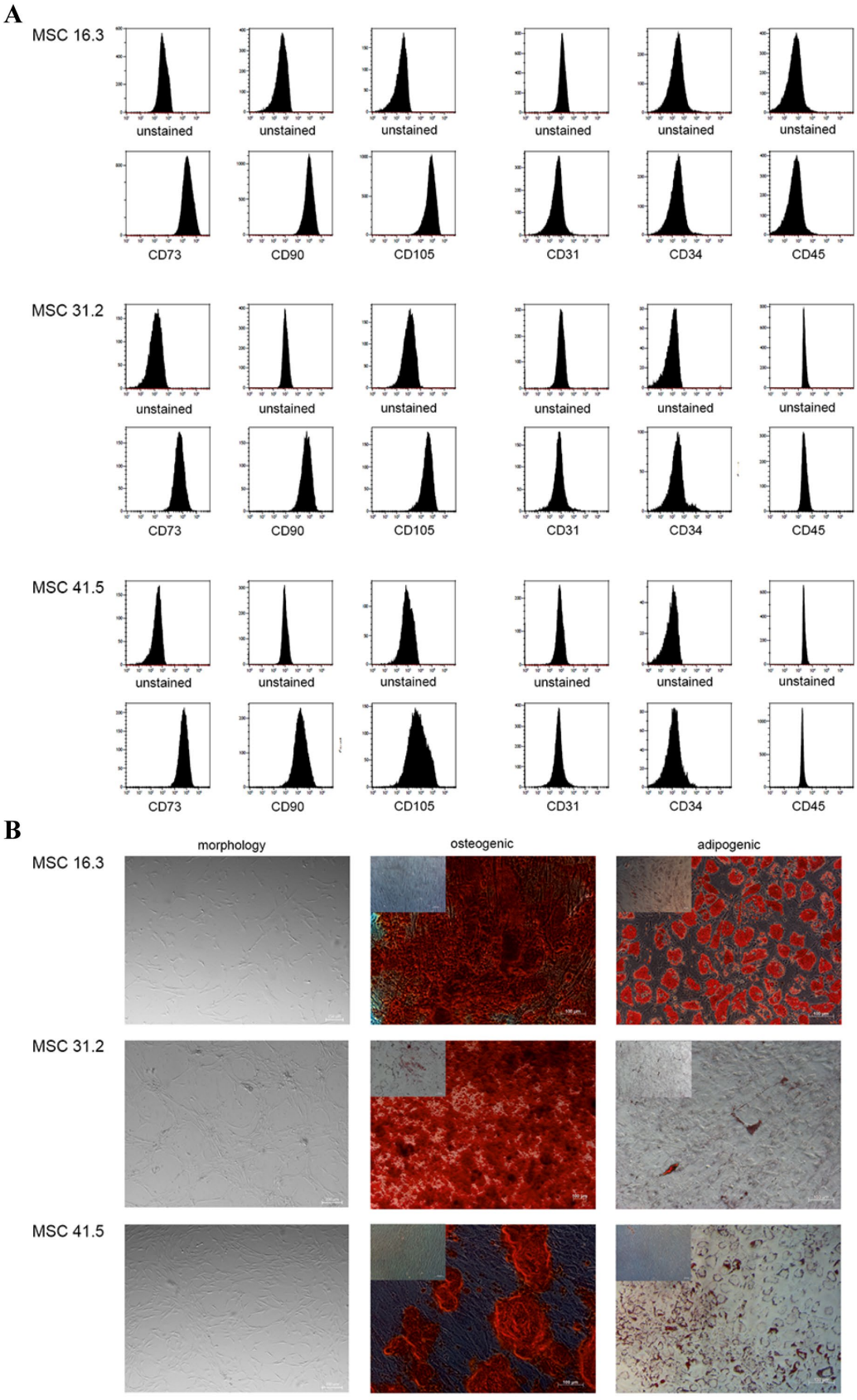

Figure 3 (for legend see page 35).

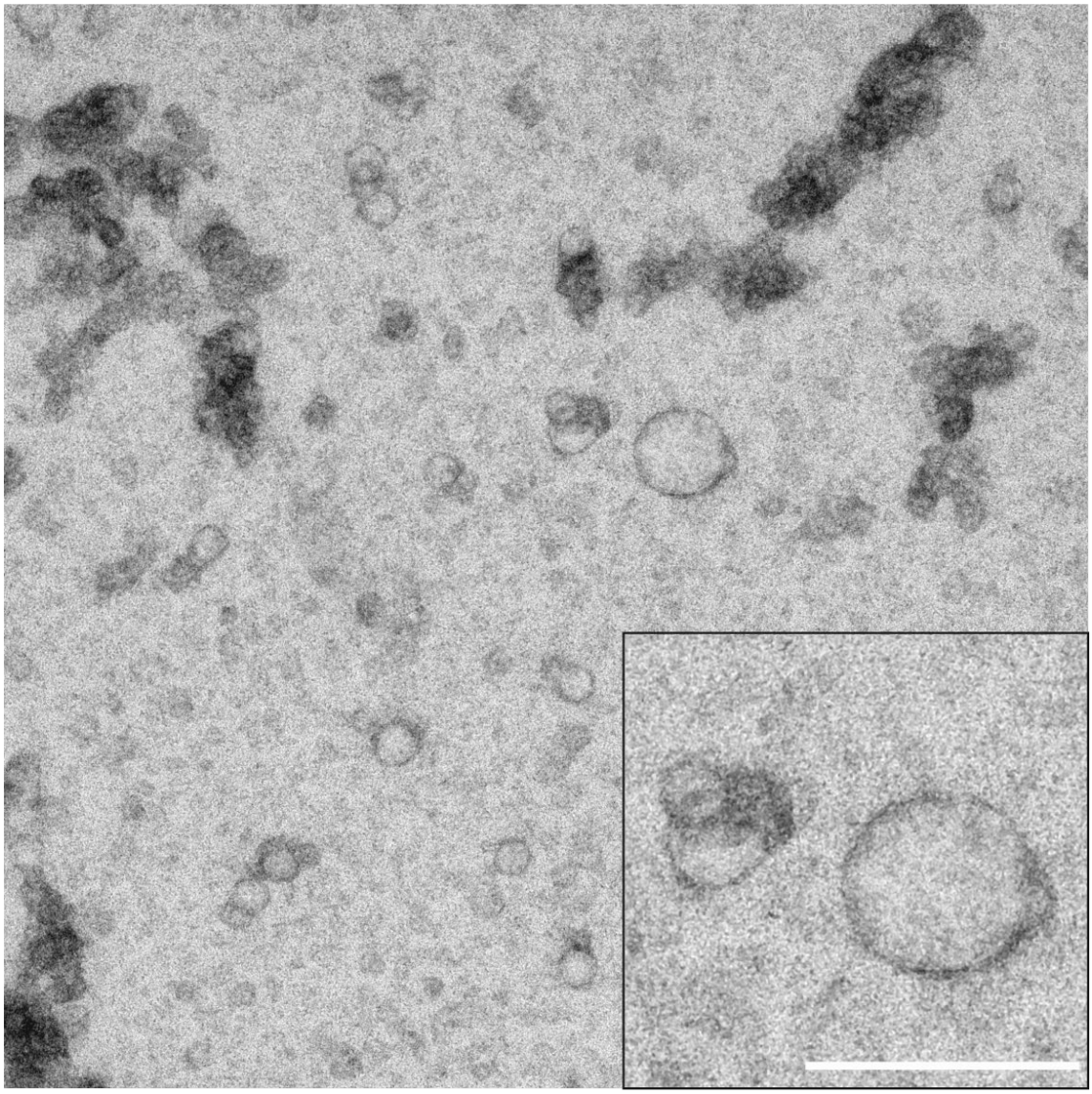

Figure 4. Transmission electron microscopy (TEM) image of a representative MSC-derived small extracellular vesicle (MSC-sEV) preparation after uranyl acetate staining. The insert reveals a magnification of the main photograph. Scale bar, 300 nm. (Data are produced by our collaborator AG Gunzer at the Institute of Experimental Immunology and Imaging, University Hospital Essen.)

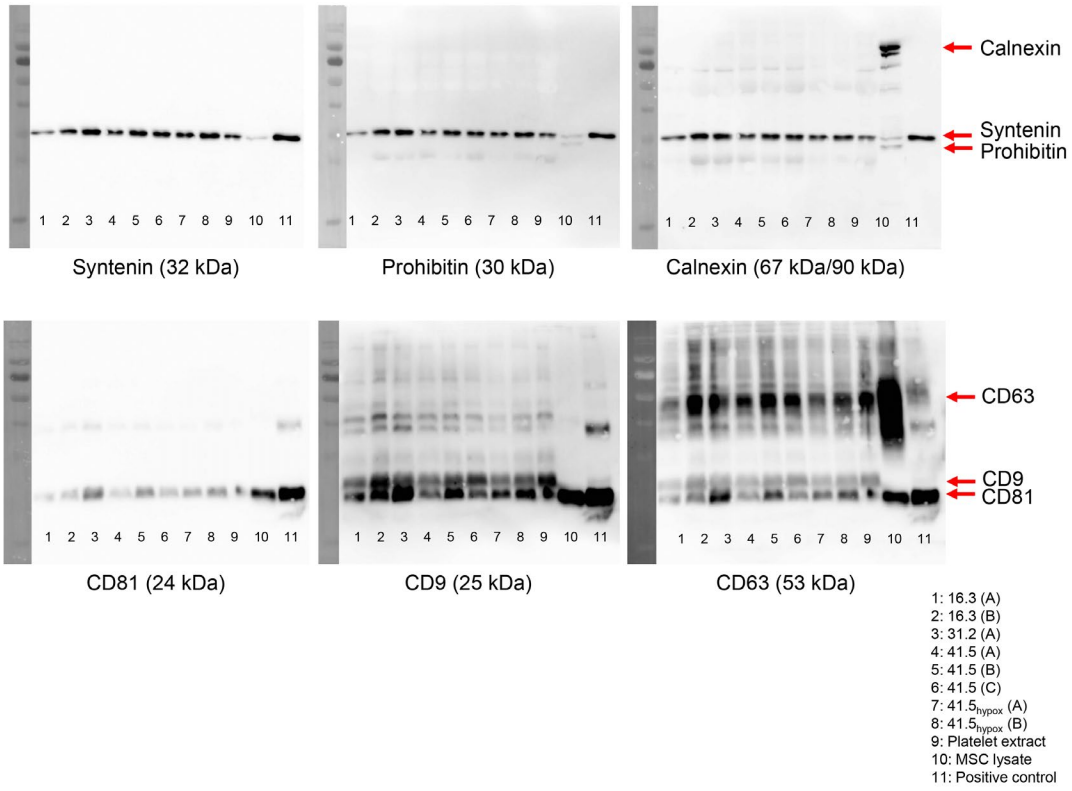

Figure 5. Characterization of MSC-sEV preparations by Western blots. All MSC-sEV preparations used within this study (1-8) contain the exosomal marker proteins syntenin, CD81, CD9, and CD63. In contrast, prohibitin and calnexin, markers for cytosolic contamination, are expressed in the cell lysate control (9) but not in any of the sEV preparations. Blots where sequentially probed with anti-syntenin, anti-prohibitin and anti-calnexin antibodies or with anti-CD81, anti-CD9 and anti-CD63 antibodies, respectively. Results after each detection round are depicted. The localization of the six proteins is indicated on the right. (Data are produced by our collaborator AG Giebel at the Institute for Transfusion Medicine, University Hospital Essen.)

4.2. MSC-sEVs attenuate neurological deficits and reduce infarct size and neuronal injury

We first evaluated MSC-sEVs obtained under regular ‘normoxic’ conditions (21% O_2 in

ambient air) and examined the heterogeneity of MSC-sEV preparations obtained from three randomly selected healthy human donors regarding their neurological recovery and tissue survival promoting effects. In mice treated with vehicle or sEV preparations obtained from these three donors (sources 16.3, 31.2 or 41.5), LDF values above the core of the middle cerebral artery territory decreased to 10-20% of baseline during MCAO followed by the recovery of LDF values to 80-90% of baseline within 15 minutes after reperfusion (**Fig. 6A**). MCAO induced reproducible neurological deficits and brain infarcts covering the striatum and most lateral cerebral cortex (**Fig. 6B and 6C**). MSC-sEV preparations from all three donors significantly attenuated neurological deficits over 72 hours post-MCAO evaluated by the Clark score, which detects both focal and global impairments (**Fig. 6B**). Conversely, infarct volume (**Fig. 6C**), the density of DNA-fragmented (i.e., irreversibly injured) TUNEL+ cells (**Fig. 6D**), and the density of DNA-fragmented TUNEL+/NeuN+ neurons (**Fig. 6E**) were significantly decreased after 72 hours by MSC-sEV preparations from two out of three donors (sources 31.2 and 41.5). In addition, serum IgG extravasation, a marker of blood-brain barrier permeability, was not influenced by any of the MSC-sEV preparations (**Fig. 6F**). These data suggest that MSC-sEV preparations induce post-ischemic neuroprotection in a donor-dependent manner.

Legend to Figure 6 (for figure see page 40). sEVs obtained from MSCs attenuate neurological deficits and induce post-ischemic neuroprotection in a donor-dependent manner. (A) Laser Doppler flow (LDF), **(B)** neurological deficits assessed by the Clark score, **(C)** infarct volume evaluated by cresyl violet staining, **(D)** DNA-fragmented cells analyzed by terminal deoxynucleotidyl transferase dUTP nick end labeling (TUNEL) staining, **(E)** neuronal injury analyzed by TUNEL/NeuN immunohistochemistry, and **(F)** extravasated serum IgG assessed at 3 days post ischemia (dpi) by immunohistochemistry in mice exposed to 30 minutes intraluminal middle cerebral artery occlusion (MCAO) followed by 72 hours survival. Vehicle or sEVs ($2x10^6$ cell equivalents in 200 µl normal saline) obtained from bone marrow MSCs of three healthy human donors (sources 16.3, 31.2, and 41.5) raised under regular conditions (21%

O_2) were intravenously administered immediately after reperfusion onset. Representative cresyl violet stainings, TUNEL, TUNEL/NeuN and IgG histochemistries are shown. Scale bar in **(C)**, 1 mm; in **(D, E)**, 100 µm; in **(F)**, 500 µm. *p<0.05, **p<0.01, ***p<0.001 (n=16-18 animals/group).

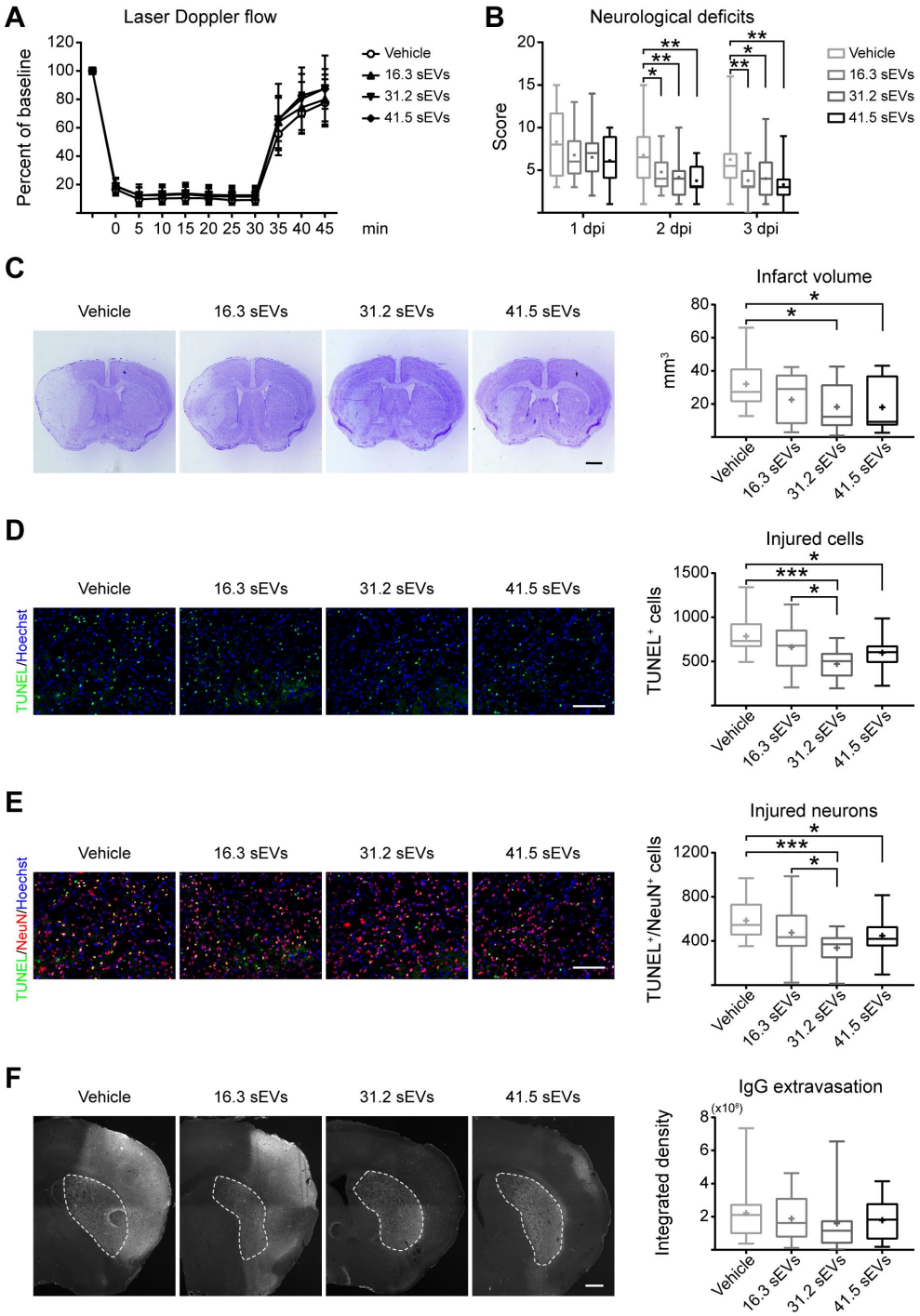

Figure 6 (for legend see page 39).

4.3. MSC-sEV induced neuroprotection is associated with reduced brain leukocyte and PMN entry

Since MSC-sEVs have been shown to have immunomodulatory effects, we next studied whether these sEV preparations affected post-ischemic brain leukocyte infiltration. The number of brain-invading CD45+ leukocytes were significantly decreased by MSC-sEVs from donor sources 31.2 and 41.5, but not from source 16.3 **(Fig. 7A)**. In order to distinguish which subtype of leukocyte is involved, we performed Ly6G immunohistochemistry for PMNs due to the fact that PMNs are the most abundant type of leukocytes and play a decisive role in post-stroke neuroinflammation. In line with the result of leukocyte infiltration, the number of brain-invading Ly6G+ PMNs was significantly reduced by MSC-sEVs from the same donor sources **(Fig. 7B)**. Note that sEVs of both donors which had neuroprotective activity in **Figure 6** (sources 31.2 and 41.5) consistently reduced brain leukocyte and PMN infiltration. In addition, the abundance of ICAM-1, an adhesion molecule that mediates, at least partly, leukocyte brain entry, was significantly decreased in the brain microvasculature by only one MSC-sEV preparation (source 31.2) (**Fig. 7C**). Since the number of PMNs in the infarcted brain peaks at an early time point, we performed additional analyses of PMN brain infiltrates at 24 hours after ischemic stroke. MSC-sEV preparations (source 41.5) in tendency reduced infarct size (**Fig. 8B**) and PMN brain infiltrates (**Fig. 8C**). Correlation analyses revealed that the number of brain PMNs was significantly associated with infarct volume (R^2=0.325, $p<0.0001$; **Fig. 9**). This R^2 value indicates that 32.5% of data variance of infarct volume were associated with PMNs. Comparative analysis of PMN brain infiltrates of mice sacrificed at 24 hours (**Fig. 8C**) and 72 hours (**Fig. 7B**) post-MCAO revealed that PMNs reached maximum levels at the earlier time-point (24 hours). These data indicate that neuroprotection by MSC-sEVs is associated with prevention of PMN brain entry.

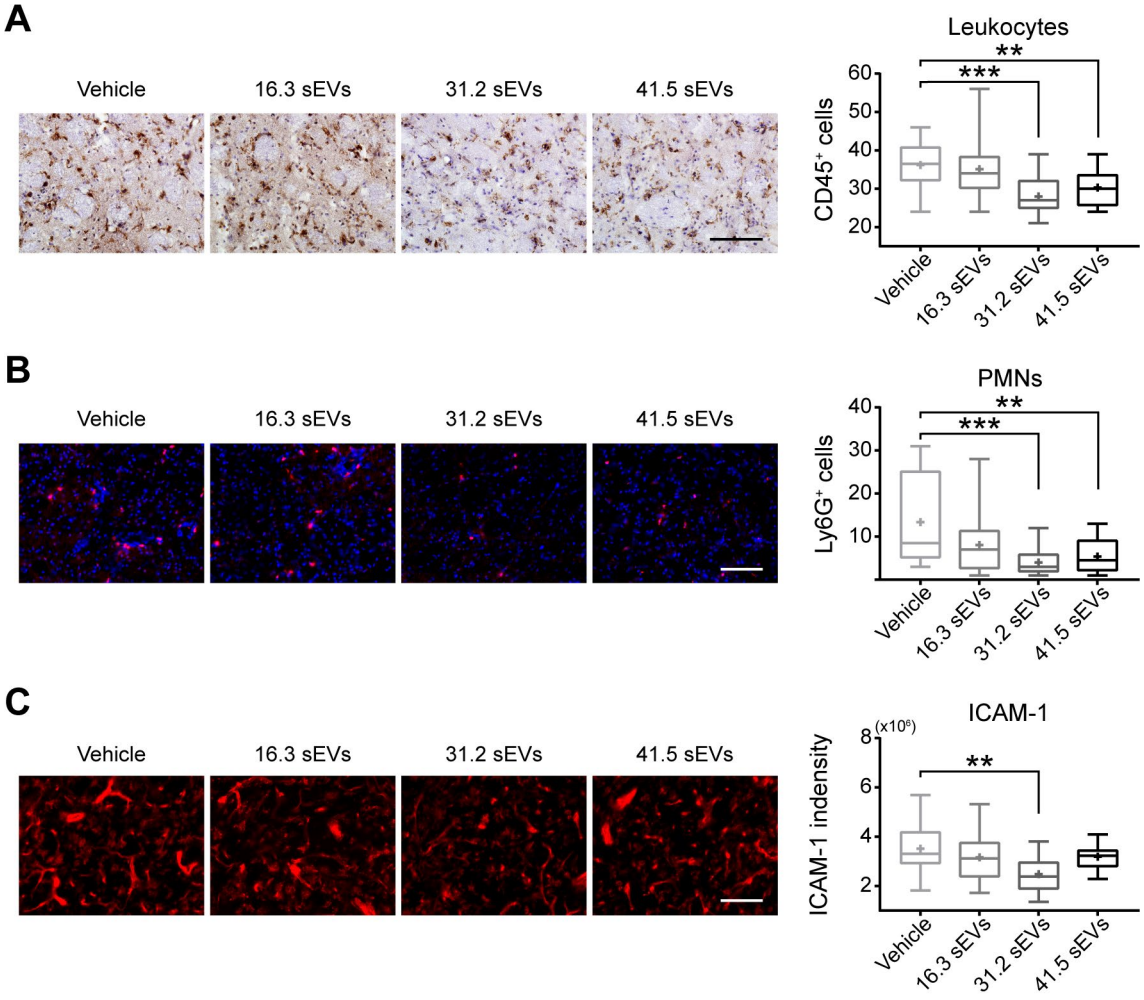

Figure 7. MSC-sEVs with neuroprotective efficacy prevent brain leukocyte and polymorphonuclear neutrophil (PMN) infiltration. (A) CD45+ leukocytes, **(B)** Ly6G+ PMN, and **(C)** ICAM-1+ microvessels assessed by immunohistochemistry in the striatal lesion of mice exposed to 30 minutes intraluminal MCAO followed by 72 hours survival. Vehicle or sEVs ($2x10^6$ cell equivalents in 200 µl normal saline) obtained from MSCs of three donors (sources 16.3, 31.2 and 41.5) raised under regular conditions (21% O_2) were intravenously applied immediately after reperfusion onset. Representative microphotographs are shown. Scale bar in **(A, B, C)**, 100 µm. **p<0.01, ***p<0.001 (n=16-18 animals/group).

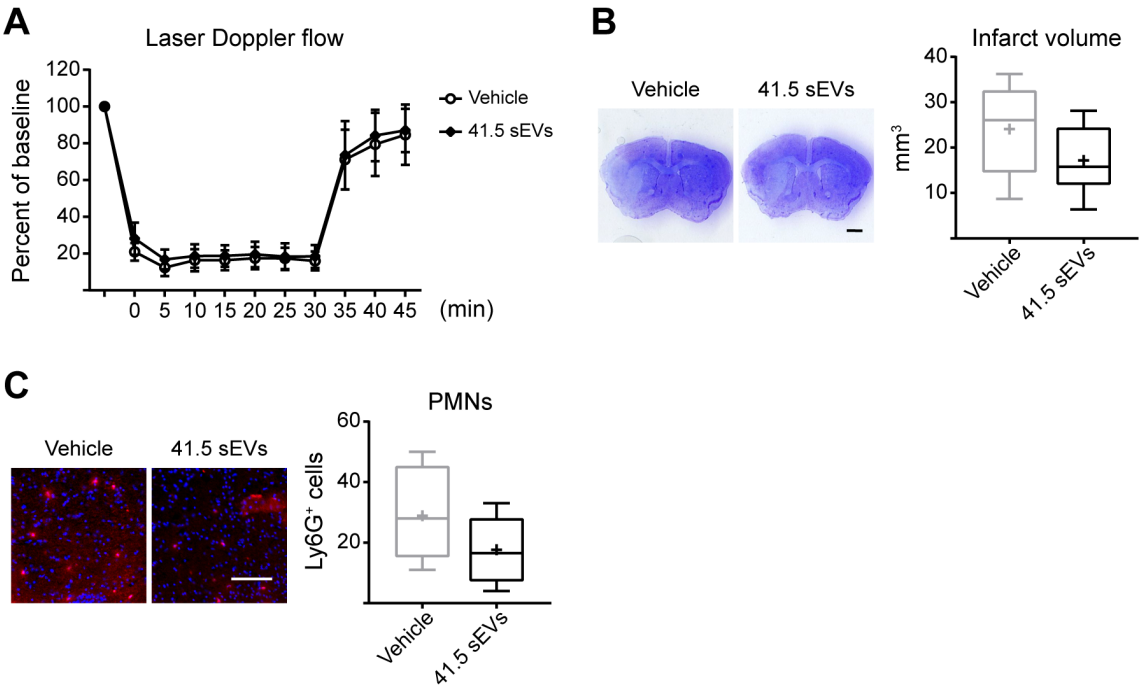

Figure 8. MSC-sEV preparations reduce brain PMN infiltrates at an early time-point. (A) LDF, **(B)** infarct volume evaluated by cresyl violet staining, and **(C)** $Ly6G^+$ PMNs in the ischemic striatum assessed by immunohistochemistry in mice exposed to 30 minutes intraluminal MCAO followed by 24 hours survival. Vehicle or sEVs ($2x10^6$ cell equivalents) obtained from conditioned medium of MSCs (source 41.5) raised under regular conditions (21% O_2, 'normoxic') were intravenously administered immediately after reperfusion. Representative cresyl violet and Ly6G stainings are shown. Scale bar in **(B)**, 1 mm; in **(C)**, 100 µm (n=7 animals/group).

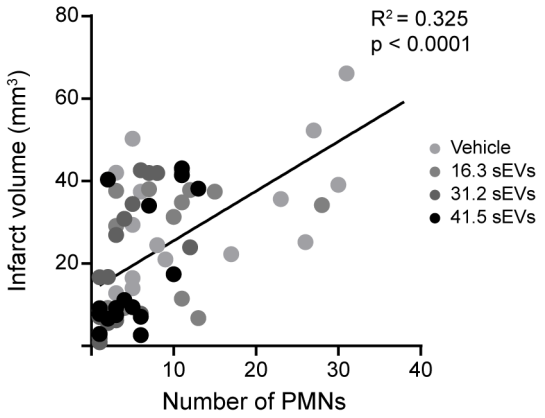

Figure 9. Brain infiltrating PMNs are tightly correlated with infarct volume. Scatter plot of number of PMNs detected in the ischemic striatum and infarct volume in mice of animal set 1 exposed to 30 minutes intraluminal MCAO followed by 72 hours survival. Vehicle or sEVs ($2x10^6$ cell equivalents) obtained from conditioned medium of independent MSCs (sources 16.3, 31.2, and 41.5) raised under regular conditions (21% O_2, 'normoxic') were intravenously administered immediately after reperfusion.

4.4. Neuroprotection by sEVs obtained under hypoxic conditions is very similar to sEVs obtained under regular 'normoxic' conditions

To investigate whether hypoxia preconditioning enhances therapeutic efficacy of MSC-sEVs in the ischemic stroke model, we next compared the MSC-sEVs collected under regular (21% O_2 in ambient air) and hypoxic (1% O_2) culture conditions. For this set of study, we used preparations from MSC source 41.5, which had been studied in other various disease models before. In mice receiving vehicle or sEVs obtained under regular or hypoxic conditions, LDF recordings again did not differ between groups (**Fig. 10A**). sEVs obtained from both culture conditions very similarly attenuated neurological deficits (**Fig. 10B**), reduced infarct volume **(Fig. 10C)**, and decreased the density of TUNEL+ injured cells **(Fig. 10D)**, TUNEL+/NeuN+ injured neurons **(Fig. 10E)**, brain-

invading CD45+ leukocytes **(Fig. 11A)** and brain-invading Ly6G+ PMNs **(Fig. 11B)**. ICAM-1 abundance was not influenced by any of the sEV preparations (**Fig. 11C**). IgG extravasation was reduced by sEVs obtained under hypoxic but not regular conditions (**Fig. 10F**), indicating preservation of blood-brain barrier integrity which was selectively induced by hypoxic sEVs.

Legend to Figure 10 (for figure see page 46). Neuroprotection by sEVs obtained from hypoxic MSCs resembles neuroprotection by sEVs obtained under regular conditions, but only sEVs from hypoxic MSCs reduce serum IgG extravasation. (A) LDF, **(B)** neurological deficits assessed by the Clark score, **(C)** infarct volume evaluated by cresyl violet staining, **(D)** DNA-fragmented cells analyzed by TUNEL staining, **(E)** neuronal injury analyzed by TUNEL/NeuN immunohistochemistry, and **(F)** extravasated serum IgG assessed by immunohistochemistry in mice exposed to 30 min MCAO followed by 72 hours survival. Vehicle or sEV preparations ($2x10^6$ cell equivalents in 200 µl normal saline) collected from MSCs (source 41.5) raised under regular (21% O_2, 'normoxic') or hypoxic (1% O_2) conditions were intravenously administered immediately after reperfusion onset. Representative cresyl violet stainings, TUNEL, TUNEL/NeuN and IgG histochemistries are shown. Scale bar in **(C)** 1 mm; in **(D, E)**, 100 µm; in **(F)**, 500 µm. *p<0.05, **p<0.01, ***p<0.001 (n=16 animals/group).

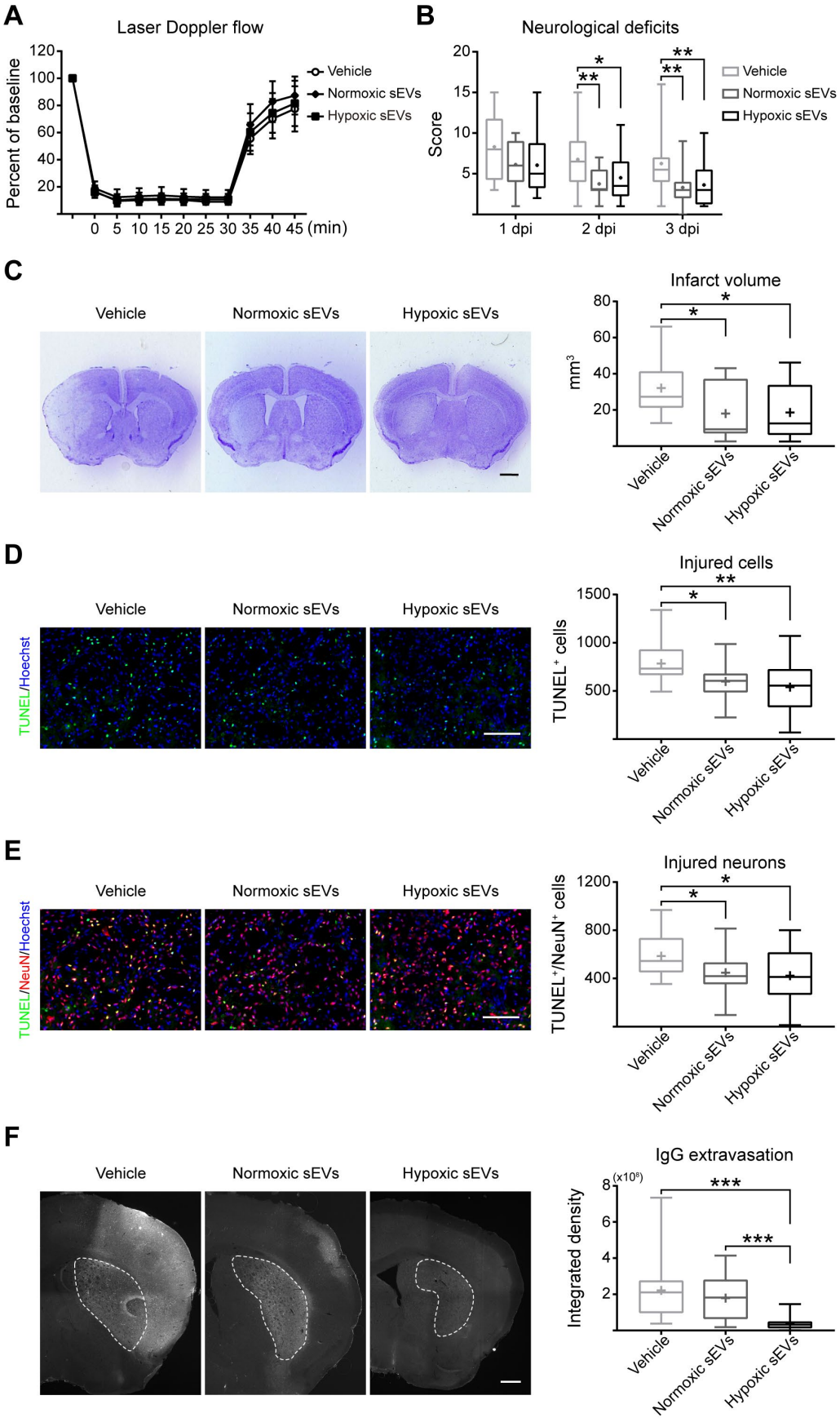

Figure 10 (for legend see page 45).

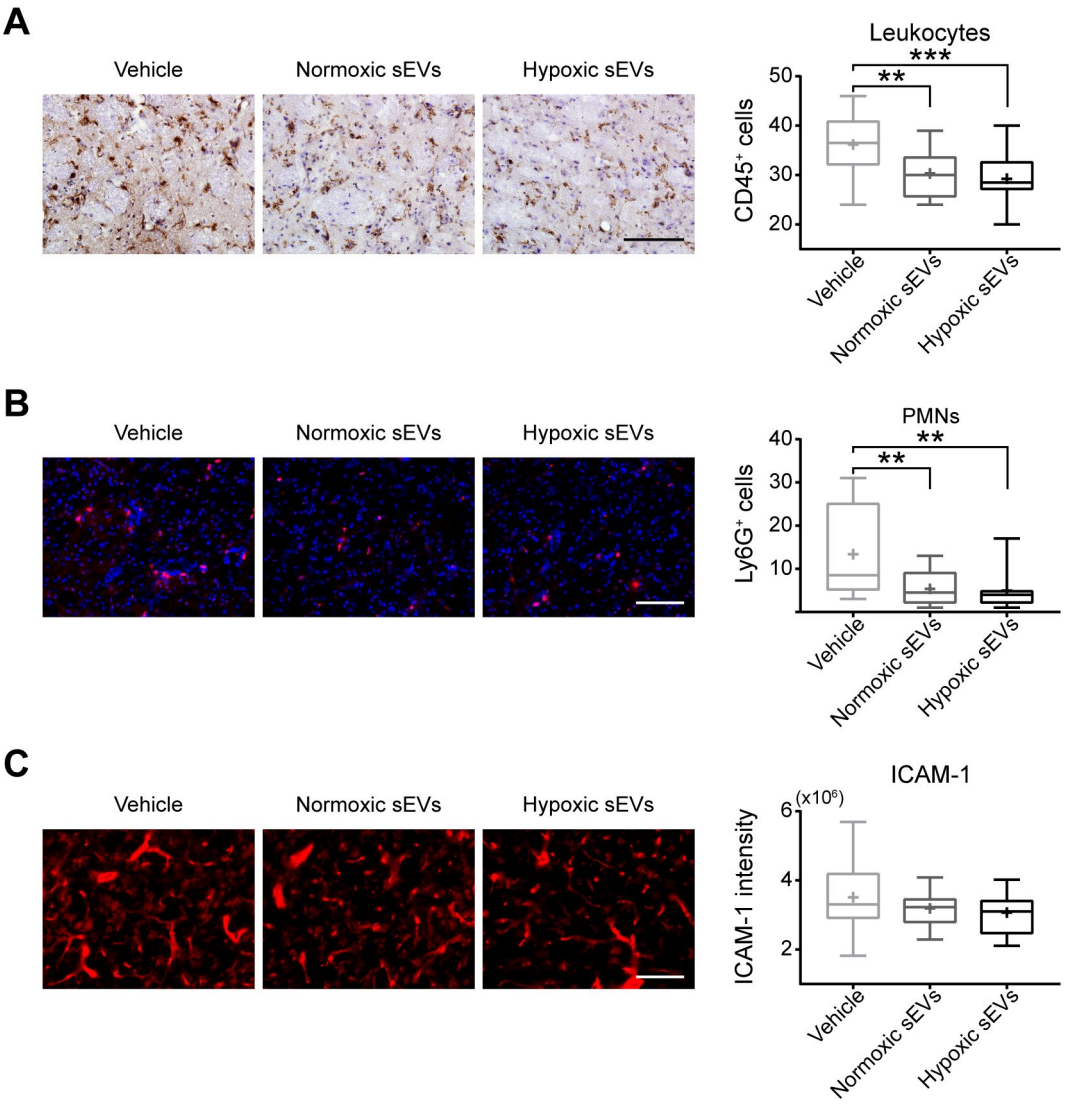

Figure 11. sEVs obtained from MSCs raised under regular and hypoxic conditions comparably reduce brain leukocyte and PMN frequencies. (A) CD45+ leukocytes, **(B)** Ly6G+ PMN, and **(C)** ICAM-1+ microvessels in the striatal lesion of mice exposed to 30 minutes intraluminal MCAO followed by 72 hours survival. Vehicle or sEV preparations ($2x10^6$ cell equivalents in 200 µl normal saline) collected from MSCs (source 41.5) under regular (21% O_2, 'normoxic') or hypoxic (1% O_2) conditions were intravenously administered immediately after reperfusion onset. Representative microphotographs are shown. Scale bar in **(A, B, C)**, 100 µm. **p<0.01, ***p<0.001 (n=16 animals/group).

4.5. PMN depletion mimics post-ischemic neuroprotection by MSC-sEVs

Based on our observation that brain PMN infiltrates correlated closely with infarct volume, considering existing knowledge that PMNs contribute to ischemic injury (Neumann et al., 2015), we next investigated the effect of PMN depletion, either alone or in combination with sEVs (source 41.5; again obtained under regular conditions at 21% O_2 or under hypoxic conditions at 1% O_2), on neurological deficits and ischemic injury. In mice exhibiting PMN depletion, which was induced by delivery of an anti-Ly6G antibody, LDF recordings did not differ from isotype IgG treated mice (**Fig. 12A, Fig. 13A**). PMN depletion mimicked the effects of sEV preparations on neurological deficits (**Fig. 12B**), infarct volume (**Fig. 12C, Fig. 13B**), the density of injured $TUNEL^+$ cells (**Fig. 12D**) and $TUNEL^+/NeuN^+$ neurons (**Fig. 12E**), and IgG extravasation (**Fig. 12F, Fig. 13C**). In PMN depleted mice, MSC-sEV administration did not reveal any additional effect on neurological deficits (**Fig. 12B**), infarct volume (**Fig. 12C, Fig. 13B**), cell injury (**Fig. 12D, E**) or IgG extravasation (**Fig. 12F, Fig. 13C**).

Legend to Figure 12 (for figure see page 49). PMN depletion by anti-Ly6G antibody mimics sEV-induced post-ischemic neuroprotection. (A) LDF, **(B)** neurological deficits assessed by the Clark score, **(C)** infarct volume evaluated by cresyl violet staining, **(D)** DNA-fragmented cells analyzed by TUNEL staining, **(E)** neuronal injury analyzed by TUNEL/NeuN histochemistry, and **(F)** extravasated serum IgG assessed by immunohistochemistry in mice exposed to 30 minutes MCAO followed by 72 hours survival. Vehicle or sEV preparations ($2x10^6$ cell equivalents in 200 µl normal saline) obtained from MSCs (source 41.5) under regular conditions (21% O_2) were intravenously administered immediately after reperfusion onset. Control (isotype) IgG or anti-Ly6G were intraperitonally applied 24 hours before and 24 hours after MCAO. Representative cresyl violet stainings, TUNEL, TUNEL/NeuN and IgG immunohistochemistries are shown. Scale bar in **(C)**, 1 mm; in **(D, E)**, 100 µm; in **(F)**, 500 µm. *$p<0.05$, **$p<0.01$ (n=14-15 animals/group).

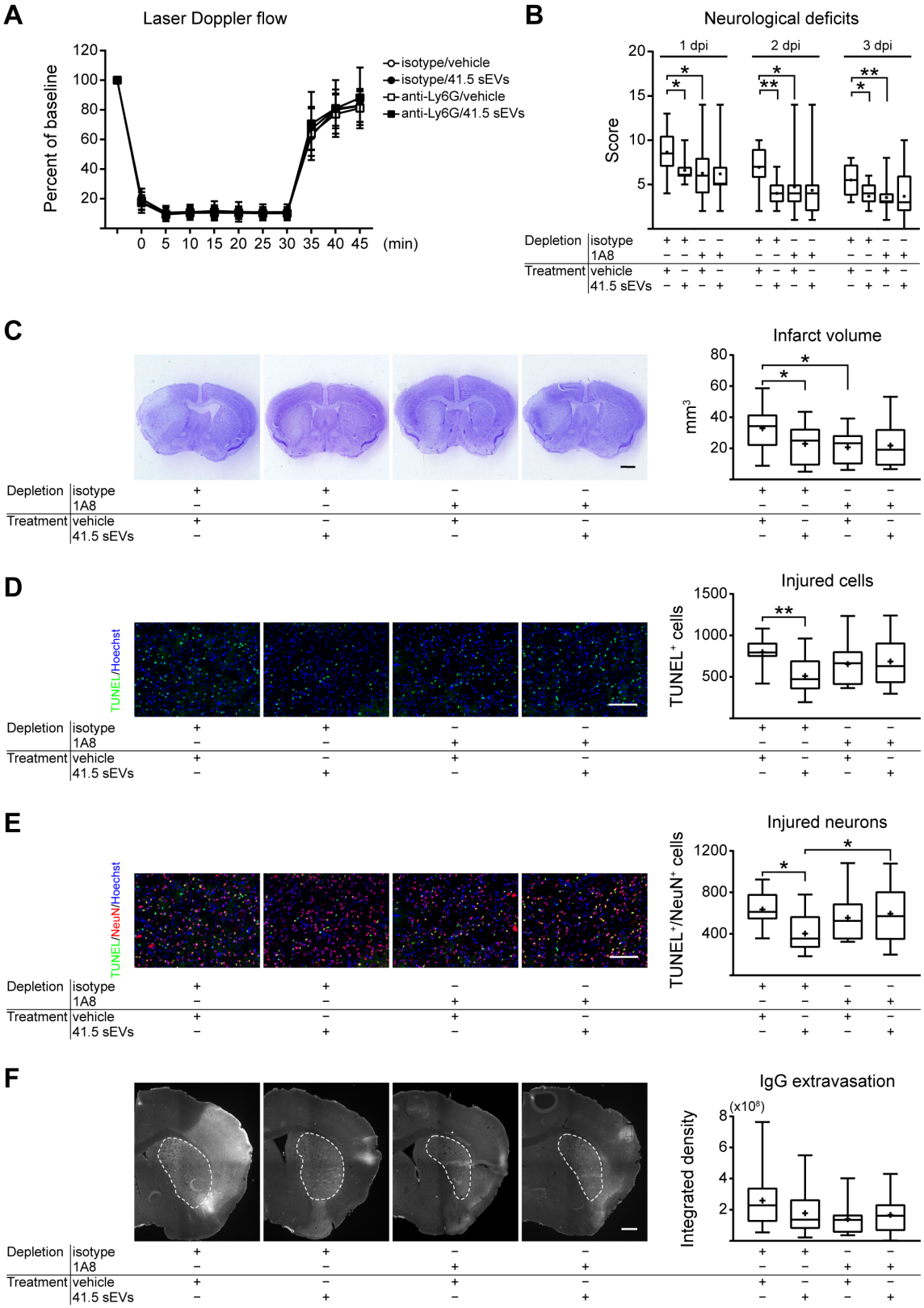

Figure 12 (for legend see page 48).

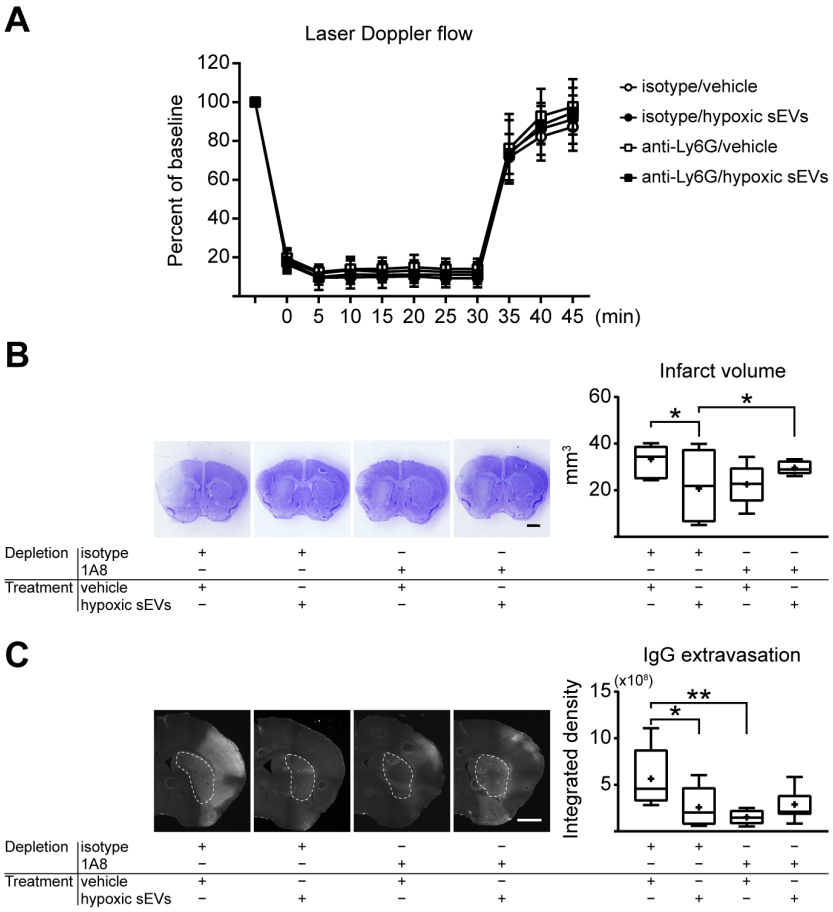

Figure 13. PMN depletion by anti-Ly6G antibody mimics post-ischemic neuroprotection induced by sEVs obtained from conditioned medium of hypoxic MSCs. (A) LDF, **(B)** infarct volume evaluated by cresyl violet staining, and **(C)** extravasated serum IgG in the ischemic striatum analyzed by immunohistochemistry in mice exposed to 30 minutes MCAO followed by 72 hours survival. Vehicle or sEV preparations ($2x10^6$ cell equivalents) obtained from conditioned medium of MSCs (source 41.5) raised under hypoxic conditions (1% O_2) were intravenously administered immediately after reperfusion. Control (isotype) IgG or anti-Ly6G (1A8) antibody were intraperitoneally applied 24 hours before and 24 hours after MCAO. Representative cresyl violet stainings and immunohistochemistries for extravasated serum IgG are shown. Note that sEVs obtained from conditioned medium of hypoxic MSCs did not reduce serum IgG extravasation in PMN depleted mice, but rather increased it. Scale bars, 1 mm. *p<0.05, **p<0.01 (n=5-7 animals/group).

4.6. PMN depletion mimics effects of MSC-sEVs on brain immune cell infiltrates

On the basis of these findings, we next evaluated the effect of PMN depletion, either alone or in combination with MSC-sEVs, on peripheral blood leukocytes and brain immune cell infiltrates. In peripheral blood of vehicle treated ischemic mice compared with vehicle treated non-ischemic mice, PMN frequencies were significantly increased and $CD4^+$ T cell, $CD8^+$ T cell and B cell frequencies were significantly reduced after 24 hours (**Figs. 14, 15**). Furthermore, PMNs were significantly activated (**Fig. 14**). In non-ischemic mice, the delivery of sEVs did not significantly influence peripheral blood frequencies and activation states of leukocytes after 24 hours (**Fig. 14**). In ischemic mice, sEV delivery significantly increased peripheral blood $CD4^+$ and $CD8^+$ T cell frequencies after 24, but not 72 hours and in tendency reduced PMN but not monocyte/ macrophage activation after 24 hours (**Figs. 14, 15**). In PMN-depleted ischemic mice, sEV delivery did not influence monocyte/ macrophage, T and B cell frequencies in peripheral blood (**Fig. 15**). In ischemic mice that were not exposed to PMN depletion, sEV administration significantly reduced the brain infiltration of leukocytes, that is, PMNs, monocytes/macrophages and B cells, after 72 hours and reduced activated microglia in ischemic brain parenchyma, as shown by immunohistochemistry or flow cytometry (**Fig. 16A, B**). These data indicated a broad anti-inflammatory action induced by MSC-sEVs. Interestingly, brain leukocyte, monocyte/macrophage and B cell, but not activated microglia counts were significantly reduced by PMN depletion (**Fig. 16B**). These results revealed that PMNs control the post-ischemic brain entry of monocytes/macrophages and lymphocytes. In PMN depleted mice, sEV delivery did not have any additional effect on brain monocyte/macrophage, lymphocyte or activated microglia counts (**Fig. 16B**). Hence, the inhibition of monocyte/macrophage and lymphocyte brain invasion by MSC-sEVs acts downstream of the prevention of PMN entry. Taken together, our data suggest a critical role of PMNs in MSC-sEV induced neuroprotection.

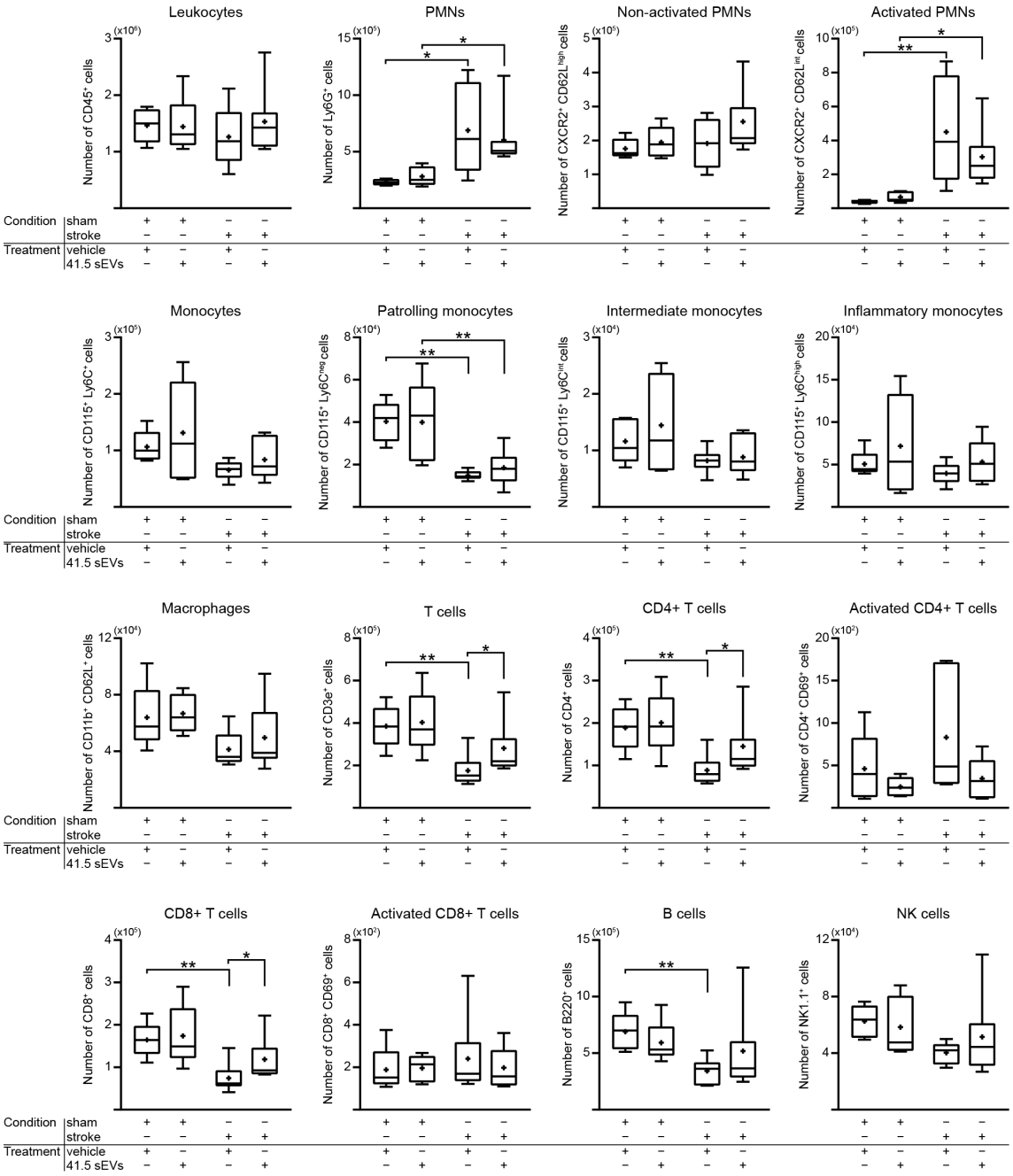

Figure 14. MSC-sEV preparations do not significantly influence PMN frequencies or PMN activation in peripheral blood at 24 hours after ischemic stroke. $CD45^+$ leukocytes, $Ly6G^+$ PMNs, $Ly6G^+$ $CXCR2^+$ $CD62L^{high}$ non-activated PMNs, $Ly6G^+$ $CXCR2^+$ $CD62L^{int}$ activated PMNs, $CD115^+$ monocytes, $CD115^+$ $Ly6C^{neg}$ patrolling monocytes, $CD115^+$ $Ly6C^{int}$ intermediate monocytes, $CD115^+$ $Ly6C^{high}$ inflammatory

monocytes, CD115^{-} CD11b^{+} CD62L^{+} macrophages, CD3e^{+} T cells, CD4^{+} T cells, CD4^{+} CD69^{+} activated T cells, CD8^{+} T cells, CD8^{+} CD69^{+} activated T cells, B220^{+} B cells, and NK1.1^{+} NK cells in peripheral blood of mice exposed to sham anesthesia or intraluminal MCAO followed by 24 hours survival assessed by flow cytometry. Vehicle or sEVs ($2x10^6$ cell equivalents) obtained from conditioned medium of MSCs (source 41.5) raised under regular conditions (21% O_2) were intravenously applied. Note the increased PMN frequencies and PMN activation and the reduced CD4^{+} and CD8^{+} T cell frequencies in ischemic compared with non-ischemic mice. MSC-sEV preparations increased T cell frequencies, but did not significantly influence PMN and monocyte frequencies or activation. *p<0.05, **p<0.01 (n=5-7 animals/group).

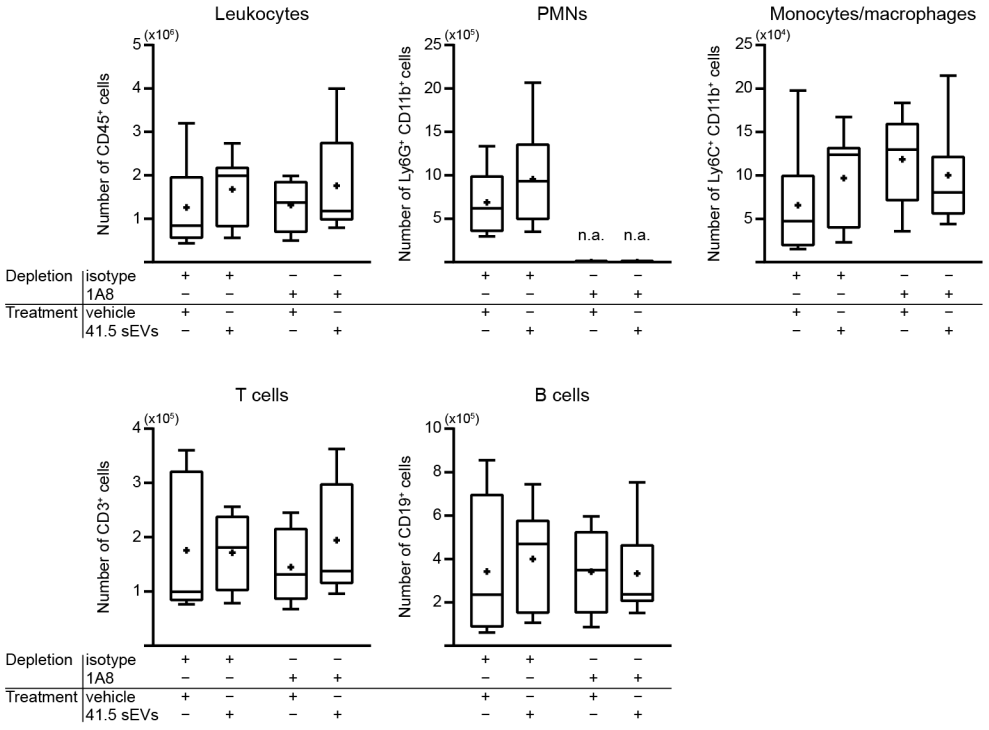

Figure 15. PMN depletion does not influence peripheral blood leukocyte frequencies at 72 hours after ischemic stroke. CD45^{+} leukocytes, Ly6G^{+} PMNs, Ly6C^{+} CD11b^{+} monocytes/macrophages, CD3^{+} T cells, and CD19^{+} B cells in peripheral blood of mice exposed to intraluminal MCAO followed by 72 hours survival assessed by flow cytometry.

Vehicle or MSC-sEVs ($2x10^6$ cell equivalents) obtained from MSCs (source 41.5) raised under regular conditions (21% O_2) were intravenously administered immediately after reperfusion. Isotype IgG or anti-Ly6G (1A8) antibody were intraperitoneally applied 24 hours before and 24 hours after MCAO. n.a., not applicable. No group differences were found (n=8-9 animals/group).

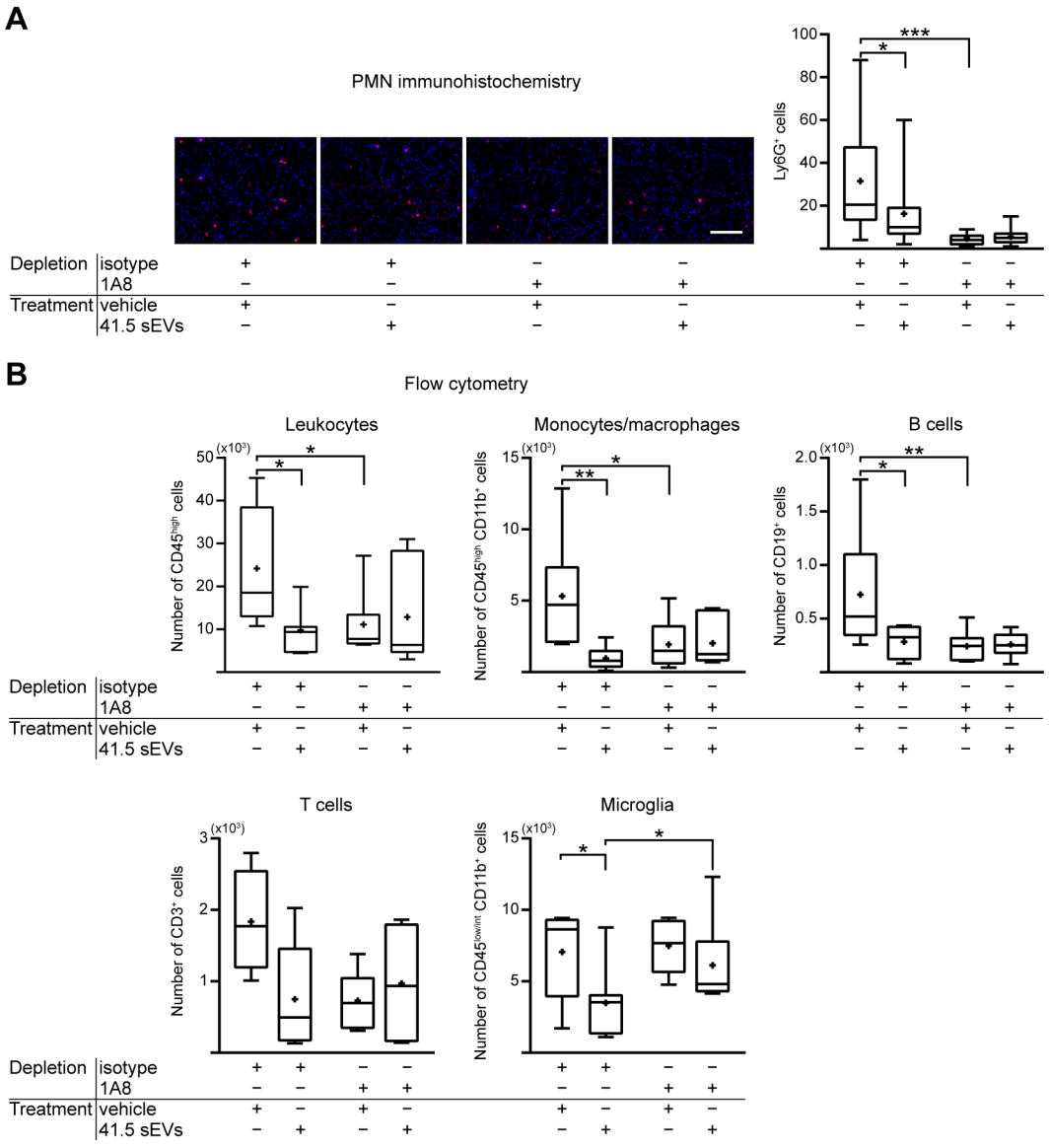

Figure 16. PMN depletion abolishes the effects of MSC-sEVs on brain infiltration of other immune cell subsets at 72 hours after ischemic stroke. (A) Density of brain-invading $Ly6G^+$ PMNs, evaluated by immunohistochemistry in the ischemic striatum, and

(B) brain invading $CD45^{high}$ leukocyte, $CD45^{high}$ $CD11b^{+}$ monocyte, $CD19^{+}$ B cell, $CD3^{+}$ T cell and $CD45^{low/int}$ $CD11b^{+}$ activated microglia counts assessed by flow cytometry in the ischemic hemisphere of mice exposed to 30 minutes MCAO followed by 72 hours survival. Vehicle or sEVs ($2x10^{6}$ cell equivalents) obtained from MSCs (source 41.5) raised under regular conditions (21% O_2) were intravenously administered immediately after reperfusion. Isotype IgG or anti-Ly6G (1A8) antibody were intraperitoneally applied 24 hours before and 24 hours after MCAO. Note that MSC-sEVs significantly reduced total leukocyte, monocyte, B cell and activated microglia counts in ischemic brains of isotype IgG treated mice. Brain leukocyte, monocyte and B cell, but not activated microglia counts were significantly reduced by PMN depletion. In PMN depleted mice, MSC-sEV administration did not have any additional effects on brain leukocyte, monocyte, B cell and activated microglia counts. Representative PMN immunohistochemistries are shown in **(A)**. Scale bar, 100 μm. *$p<0.05$, **$p<0.01$, ***$p<0.001$ (n=7-8 animals/group).

5. DISCUSSION

We herein show that MSC-derived sEVs induce post-ischemic neuroprotection, when administered in the acute stroke phase in mice exposed to intraluminal MCAO. For evaluating MSC-sEV heterogeneity, we examined sEV preparations obtained from three randomly selected healthy human MSC donors (sources 16.3, 31.2 and 41.5). MSC-sEV preparations of all three donors significantly reduced neurological deficits. However, only two preparations of these donors (sources 31.2 and 41.5) in addition reduced infarct volume and neuronal injury. Structural neuroprotection by these two sEV preparations consistently went along with reduced brain infiltration of PMNs, monocytes/macrophages and lymphocytes and reduced microglial activation. The neuroprotective efficacy of sEVs obtained from hypoxic MSCs (source 41.5) was similar to that of sEVs from normoxic MSCs (again source 41.5), but sEVs from hypoxic MSCs also stabilized blood-brain barrier integrity indicated by reduced serum IgG extravasation. In addition, PMN depletion mimicked the effects of MSC-sEVs on neurological recovery, ischemic injury and brain PMN, monocyte and lymphocyte counts. However, combined PMN depletion and MSC-sEV administration did not have any synergistic effects superior to sole PMN depletion in any of the readouts examined, indicating that PMNs play a central role in the MSC-sEV-induced post-ischemic neuroprotection.

Our data show that sEVs derived from donor sources 31.2 and 41.5, but not from source 16.3, exerted structural neuroprotection, suggesting that the neuroprotective efficacy of MSC-sEVs can vary between individual preparations. The heterogeneity of MSC-sEVs may be largely inherited from their parental MSCs. In fact, MSCs have been reported to be intrinsically and functionally heterogeneous, which has been highly ascribed to the inconsistent outcomes between MSC-based clinical trials (Phinney, 2012). For instance, since a landmark case report in 2004 described the success of haploidentical MSC infusion in treating a child with severe treatment-resistant grade IV acute graft-versus-host disease (GvHD) (Le Blanc et al., 2004) and a series of subsequent phase II

clinical trials showed positive results of MSCs for treatment of GvHD (Bernardo et al., 2011; Le Blanc et al., 2008; Peng et al., 2015; Ringden et al., 2006), MSCs have become an attractive promising therapeutic strategy for treating GvHD. However, a later phase III clinical trial (NCT00366145) reported negative results in examining the use of MSCs for steroid-refractory GvHD (Martin et al., 2010). These conflicting trial outcomes can be explained by the intrinsic heterogeneity of MSCs coupled with not sufficiently standardized manufacturing protocols (Galipeau, 2013; Phinney, 2012). To our best knowledge, the present study is the first to evaluate and clearly show MSC-sEV heterogeneity in a mouse model of ischemic stroke. Although a recently published phase I/II study reported promising results of intravenous transfusion of allogeneic MSCs in terms that MSC delivery was safe in patients with chronic stroke (Levy et al., 2019), we urgently need to develop functional assays that allow predicting the efficacy of MSC-sEVs before clinical trials are initiated.

Under conditions associated with neuroprotection, reduced brain PMN infiltrates might represent a surrogate of decreased brain injury rather than a causative event mediating tissue survival. Thus, we explored consequences of PMN depletion on neuroprotective effects of MSC-sEVs. Using anti-Ly6G delivery, we now showed that PMN depletion mimics the effects of MSC-sEVs on neurological deficits, infarct volume and neuronal injury, as well as on brain monocyte/macrophage and lymphocyte infiltrates. In PMN depleted mice, MSC-sEVs notably did not have any additional effect on infarct volume and neuronal injury, and brain monocyte/macrophage and lymphocyte counts were not further attenuated by MSC-sEVs. PMNs have long been believed and recently been proven to contribute to ischemic injury after intraluminal MCAO (Hermann and Gunzer, 2019). Using the same strategy, i.e., anti-Ly6G or anti-Gr1 mediated PMN depletion, we have previously demonstrated that depletion of PMNs alone provides a degree of neuroprotection that cannot further be amplified when the brain entry of additional immune cell subsets (e.g., T cells, B cells and monocytes) is prevented by anti-VLA4 (very late antigen-4) (Hermann and Gunzer, 2019; Neumann et al., 2015). By

showing that PMN depletion reduces the brain accumulation of various immune cell subsets (i.e., monocytes and lymphocytes) in the ischemic brain, we now provide a likely possible explanation for their profound influence of PMNs on ischemic injury. PMN depletion has previously been shown to reduce the brain infiltration of monocytes in a mouse model of intracerebral hemorrhage (Sansing et al., 2011) and to decrease microglial activation in a mouse model of traumatic brain injury (Kenne et al., 2012). The observation that PMN depletion prevents the brain accumulation of monocytes and lymphocytes in the ischemic brain is new. Our data indicate that PMNs play a decisive role in MSC-sEV-induced neuroprotection.

We have previously shown that MSC-sEV administration 24 hours after MCAO reverses post-ischemic lymphopenia in the peripheral blood at 6 days post stroke (Doeppner et al., 2015). We herein confirmed that MSC-sEVs reverse post-ischemic lymphopenia. The here-presented study differs from this previous study in that we administered MSC-sEVs immediately after reperfusion onset and examined lymphopenia after 24 hours. This study reveals that MSC-sEVs modulate immune responses in an early injury phase. Notably, MSC-sEV delivery did not significantly influence PMN frequencies and PMN activation in peripheral blood, neither in the present nor the previous study (Doeppner et al., 2015). Since ICAM-1, a cell adhesion molecule involved in leukocyte brain entry, was largely unaffected by MSC-sEVs, the precise mechanism via which MSC-sEVs prevented brain PMN invasion, remains to be determined. Reduction of PMN tissue infiltrates by MSC-sEVs has previously been shown in rat and mouse models of traumatic and inflammatory lung injuries (Li et al., 2019; Zhu et al., 2014). That MSC-sEVs attenuate PMN infiltrates in the brain tissue has to the best of our knowledge not been shown.

The modification of PMNs by MSC-sEVs opens promising perspectives for clinical translation. Due to peripheral infection (e.g., pneumonia or sepsis) risks, we will not be able to deplete PMNs in human stroke patients, albeit they undoubtedly contribute to ischemic injury (Hermann and Gunzer, 2019). Since MSC-sEVs did not significantly

affect PMN frequencies or activation in the peripheral blood and MSC-sEVs specifically targeted and accumulated in the pathological brain regions of murine models of neurological disorders (Perets et al., 2019), we might be able to antagonize the detrimental effects of PMNs related to their accumulation in the brain parenchyma without interfering with peripheral immune responses. Concerted efforts are needed in the development of assays that allow predicting the biological activity and clinical efficacy of MSC-sEVs.

In summary, we show that compared to mice receiving vehicle injections, immune cell infiltrates are reduced after focal cerebral ischemia by MSC-derived sEVs resulting in structural protection of the ischemic brain (**Figure 17**). Similar to MSC-sEV treatment, the depletion of PMNs by anti-Ly6G antibody delivery reduces post-ischemic immune cell infiltrates, providing post-ischemic neuroprotection in a way resembling MSC-sEVs (**Figure 17**). In animals exhibiting PMN depletion, MSC-sEV delivery does not have any additive effect to PMN depletion, neither with respect to brain immune cell infiltrates, nor its neuroprotective effect (**Figure 17**). Our study reveals that PMNs are important effectors mediating the effects of MSC-sEVs on brain immune cell infiltrates other than PMNs and ischemic brain injury.

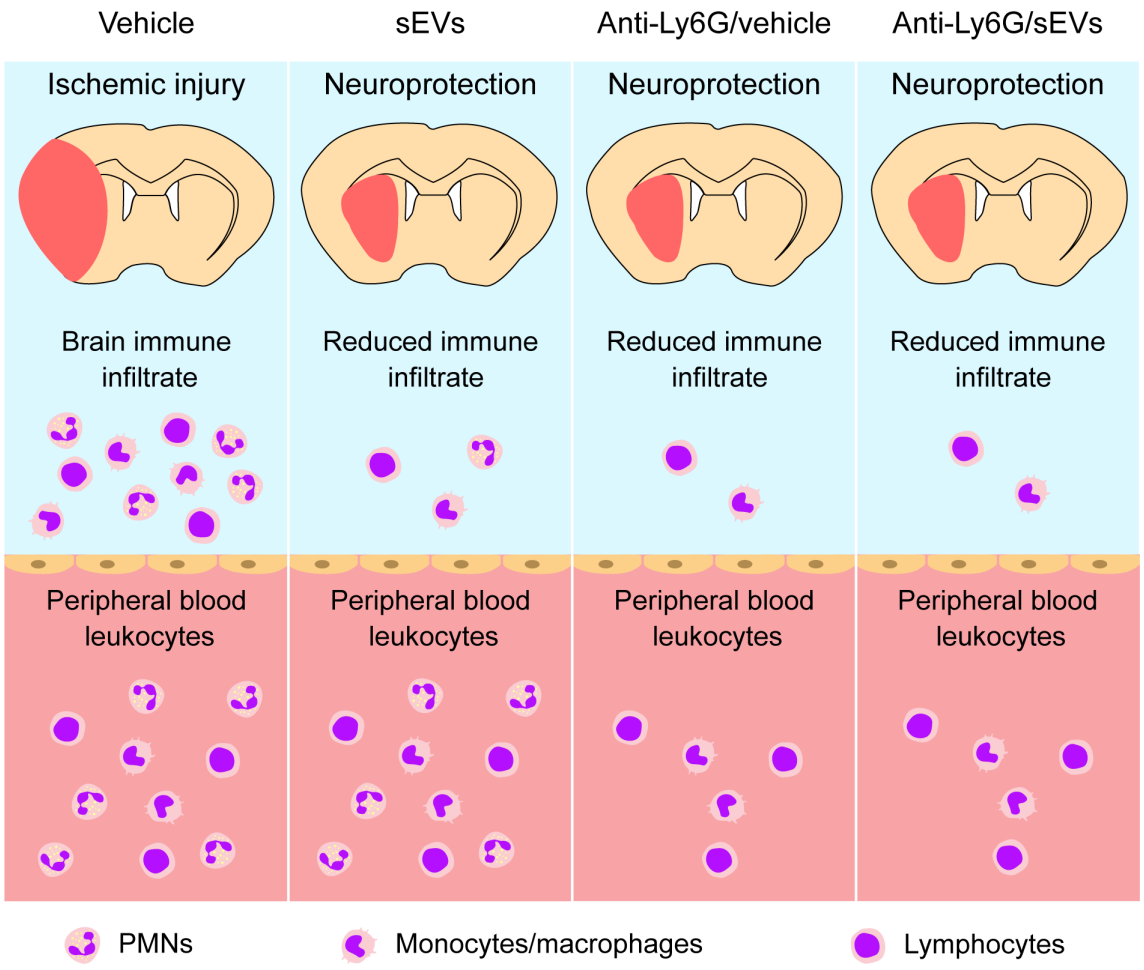

Figure 17. Visual summary: Role of brain-invading leukocytes and, specifically, PMNs in post-ischemic neuroprotection induced by MSC-derived sEV preparations. In ischemic brains not receiving MSC-sEVs, peripheral blood leukocytes that include PMNs enter the brain, resulting in brain injury. MSC-sEV preparations reduce brain infiltrates of PMNs, monocytes/ macrophages and lymphocytes. PMN depletion also decreases brain infiltrates of PMNs, monocytes/ macrophages and lymphocytes. As a consequence of the reduced brain leukocyte infiltrates, neuroprotection is noted.

6. SUMMARY

Small extracellular vesicles (sEVs) obtained from mesenchymal stromal cells (MSCs) were shown to induce neurological recovery after focal cerebral ischemia in rodents and to reverse post-ischemic lymphopenia in peripheral blood. Since peripheral blood cells, especially polymorphonuclear neutrophils (PMNs), contribute to ischemic brain injury, we analyzed brain leukocyte responses to sEVs and investigated the role of PMNs in sEV-induced neuroprotection.

Male C57Bl6/j mice were exposed to transient intraluminal middle cerebral artery occlusion. After reperfusion onset, vehicle or sEVs prepared from conditioned media of MSCs raised from bone marrow (BM) samples of three randomly selected healthy human donors were intravenously administered. sEVs obtained from normoxic and hypoxic MSCs were applied. PMNs were depleted in vehicle and MSC-sEV treated mice. Neurological deficits, ischemic injury, blood-brain barrier integrity, peripheral blood leukocyte responses and brain leukocyte infiltration were evaluated over 72 hours.

sEV preparations of all three donors collected from normoxic MSCs significantly reduced neurological deficits. Preparations of two of these donors significantly decreased infarct volume and neuronal injury. sEV-induced neuroprotection was consistently associated with decreased brain infiltrates of leukocytes, namely of PMNs, monocytes/ macrophages and lymphocytes. sEVs obtained from hypoxic MSCs (1% O_2) had very similar effects on neurological deficits and ischemic injury as MSC-sEVs obtained under regular conditions (21% O_2), but also reduced serum IgG extravasation, a marker of blood-brain barrier permeability. PMN depletion mimicked the effects of MSC-sEVs on neurological recovery, ischemic injury and brain PMN, monocyte and lymphocyte counts. Combined MSC-sEV administration and PMN depletion did not have any effects superior to PMN depletion alone in any of the readouts examined.

Leukocytes and specifically PMNs contribute to MSC-sEV induced post-ischemic neuroprotection. Individual MSC-sEV preparations may differ in their neuroprotective activities. Thus, potency assays are urgently needed to identify their therapeutic efficacy before clinical application.

ZUSAMMENFASSUNG

Es wurde bislang gezeigt, dass kleine extrazelluläre Vesikel (sEVs) von mesenchymalen Stromazellen (MSCs), nach einer fokalen zerebralen Ischämie in Nagetieren neuroprotektiv wirken und einer post-ischämischen Lymphopenie entgegenwirken. Da periphere Blutzellen, insbesondere polymorphkernige Neutrophile (PMNs), zur ischämischen Gehirnschädigung beitragen, wurden die Auswirkungen von sEVs auf Leukozyten untersucht und die Rolle von PMNs in sEV-induzierter Protektion analysiert.

Männliche C57Bl6/j Mäuse wurden einer intraluminalen Okklusion der mittleren Zerebralarterie ausgesetzt. Mit Beginn der Reperfusion wurden entweder Vehikel oder sEVs, isoliert aus konditioniertem Medium von Knochenmark-MSCs von drei gesunden und zufälligen menschlichen Spendern, intravenös injiziert. Es wurden sEVs von normoxischen oder hypoxischen MSCs verwendet. PMNs wurden in den Vehikel- oder MSC-sEV-behandelten Mäusen depletiert. Über einen Zeitraum von 72 Stunden wurden neurologische Defizite, die ischämische Schädigung, die Blut-Hirn-Schrankenintegrität, periphere Leukozyten und die Leukozyteninfiltration untersucht.

sEVs aus normoxischen MSCs aller drei Spender reduzierten signifikant neurologische Defizite. sEVs von MSCs zweier Spender verringerten signifikant das Infarktvolumen und die neurologische Schädigung. Die sEV-induzierte Neuroprotektion war assoziiert mit einer niedrigeren Leukozyteninfiltration, insbesondere von PMNs, Monozyten/ Makrophagen und Lymphozyten. sEVs aus hypoxischen MSCs (1% O_2) hatten ähnliche Effekte auf neurologische Defizite und die ischämische Schädigung wie MSC-sEVs, die unter regulären Bedingungen (21% O_2) isoliert wurden, aber verringerten auch die Extravasation von Serum IgG. Die Depletion von PMNs hatte eine vergleichbare Auswirkung auf die neurologische Erholung, die ischämische Schädigung und die Zahl der PMNs, Monozyten und Lymphozyten im Gehirn, wie MSC-sEVs. Die Applikation von MSC-sEVs in Kombination mit einer PMN Depletion verbesserte die Wirkung der alleinigen PMN Depletion, bezogen auf die untersuchten Parameter, nicht zusätzlich.

Leukozyten, insbesondere PMNs, tragen zur MSC-sEV-induzierten post-ischämischen Neuroprotektion bei. Individuelle MSC-sEV Fraktionen unterscheiden sich u.U. hinsichtlich ihres neuroprotektiven Potentials. Die Entwicklung von Aktivitätsassays, die geeignet sind das therapeutische Potential einzuschätzen, ist daher vor einer klinischen Applikation zwingend notwendig.

7. REFERENCES

1. Akopov, S.E., Simonian, N.A., and Grigorian, G.S. (1996). Dynamics of polymorphonuclear leukocyte accumulation in acute cerebral infarction and their correlation with brain tissue damage. Stroke *27*, 1739-1743.

2. Ankrum, J.A., Ong, J.F., and Karp, J.M. (2014). Mesenchymal stem cells: immune evasive, not immune privileged. Nat Biotechnol *32*, 252-260.

3. Baldari, S., Di Rocco, G., Piccoli, M., Pozzobon, M., Muraca, M., and Toietta, G. (2017). Challenges and Strategies for Improving the Regenerative Effects of Mesenchymal Stromal Cell-Based Therapies. Int J Mol Sci *18*, 2087.

4. Benjamin, E.J., Muntner, P., Alonso, A., Bittencourt, M.S., Callaway, C.W., Carson, A.P., Chamberlain, A.M., Chang, A.R., Cheng, S., Das, S.R., Delling, F.N., Djousse, L., Elkind, M.S.V., Ferguson, J.F., Fornage, M., Jordan, L.C., Khan, S.S., Kissela, B.M., Knutson, K.L., Kwan, T.W., Lackland, D.T., Lewis, T.T., Lichtman, J.H., Longenecker, C.T., Loop, M.S., Lutsey, P.L., Martin, S.S., Matsushita, K., Moran, A.E., Mussolino, M.E., OFlaherty, M., Pandey, A., Perak, A.M., Rosamond, W.D., Roth, G.A., Sampson, U.K.A., Satou, G.M., Schroeder, E.B., Shah, S.H., Spartano, N.L., Stokes, A., Tirschwell, D.L., Tsao, C.W., Turakhia, M.P., VanWagner, L.B., Wilkins, J.T., Wong, S.S., and Virani, S.S. (2019). Heart Disease and Stroke Statistics-2019 Update: A Report From the American Heart Association. Circulation *139*, e56-e528.

5. Bernardo, M.E., Ball, L.M., Cometa, A.M., Roelofs, H., Zecca, M., Avanzini, M.A., Bertaina, A., Vinti, L., Lankester, A., Maccario, R., Ringden, O., Le Blanc, K., Egeler, R.M., Fibbe, W.E., and Locatelli, F. (2011). Co-infusion of ex vivo-expanded, parental MSCs prevents life-threatening acute GVHD, but does not reduce the risk of graft failure in pediatric patients undergoing allogeneic umbilical cord blood transplantation. Bone Marrow Transplant *46*, 200-207.

6. Börger, V., Bremer, M., Ferrer-Tur, R., Gockeln, L., Stambouli, O., Becic, A., and Giebel, B. (2017). Mesenchymal Stem/Stromal Cell-Derived Extracellular Vesicles and

Their Potential as Novel Immunomodulatory Therapeutic Agents. Int J Mol Sci *18*, 1450.

7. Chamorro, A., Meisel, A., Planas, A.M., Urra, X., van de Beek, D., and Veltkamp, R. (2012). The immunology of acute stroke. Nat Rev Neurol *8*, 401-410.

8. Chen, J., Li, Y., Wang, L., Zhang, Z., Lu, D., Lu, M., and Chopp, M. (2001). Therapeutic benefit of intravenous administration of bone marrow stromal cells after cerebral ischemia in rats. Stroke *32*, 1005-1011.

9. Clark, W.M., Lessov, N.S., Dixon, M.P., and Eckenstein, F. (1997). Monofilament intraluminal middle cerebral artery occlusion in the mouse. Neurol Res *19*, 641-648.

10. Collino, F., Lopes, J.A., Correa, S., Abdelhay, E., Takiya, C.M., Wendt, C.H.C., de Miranda, K.R., Vieyra, A., and Lindoso, R.S. (2019). Adipose-Derived Mesenchymal Stromal Cells Under Hypoxia: Changes in Extracellular Vesicles Secretion and Improvement of Renal Recovery after Ischemic Injury. Cell Physiol Biochem *52*, 1463-1483.

11. Cui, G.H., Wu, J., Mou, F.F., Xie, W.H., Wang, F.B., Wang, Q.L., Fang, J., Xu, Y.W., Dong, Y.R., Liu, J.R., and Guo, H.D. (2018). Exosomes derived from hypoxia-preconditioned mesenchymal stromal cells ameliorate cognitive decline by rescuing synaptic dysfunction and regulating inflammatory responses in APP/PS1 mice. FASEB J *32*, 654-668.

12. Doeppner, T.R., Herz, J., Gorgens, A., Schlechter, J., Ludwig, A.K., Radtke, S., de Miroschedji, K., Horn, P.A., Giebel, B., and Hermann, D.M. (2015). Extracellular Vesicles Improve Post-Stroke Neuroregeneration and Prevent Postischemic Immunosuppression. Stem Cells Transl Med *4*, 1131-1143.

13. Dominici, M., Le Blanc, K., Mueller, I., Slaper-Cortenbach, I., Marini, F., Krause, D., Deans, R., Keating, A., Prockop, D., and Horwitz, E. (2006). Minimal criteria for defining multipotent mesenchymal stromal cells. The International Society for Cellular Therapy position statement. Cytotherapy *8*, 315-317.

14. Drummond, J.C., Piyash, P.M., and Kimbro, J.R. (2000). Neuroprotection failure in stroke. The Lancet *356*, 1032-1033.

15. El Andaloussi, S., Mäger, I., Breakefield, X.O., and Wood, M.J.A. (2013). Extracellular vesicles: biology and emerging therapeutic opportunities. Nat Rev Drug Discov *12*, 347.

16. Elkins, J., Veltkamp, R., Montaner, J., Johnston, S.C., Singhal, A.B., Becker, K., Lansberg, M.G., Tang, W., Chang, I., Muralidharan, K., Gheuens, S., Mehta, L., and Elkind, M.S.V. (2017). Safety and efficacy of natalizumab in patients with acute ischaemic stroke (ACTION): a randomised, placebo-controlled, double-blind phase 2 trial. The Lancet Neurol *16*, 217-226.

17. Enlimomab Acute Stroke Trial Investigators (2001). Use of anti-ICAM-1 therapy in ischemic stroke: results of the Enlimomab Acute Stroke Trial. Neurology *57*, 1428-1434.

18. Evans, M.R.B., White, P., Cowley, P., and Werring, D.J. (2017). Revolution in acute ischaemic stroke care: a practical guide to mechanical thrombectomy. Pract Neurol *17*, 252-265.

19. Ferguson, S.W., and Nguyen, J. (2016). Exosomes as therapeutics: The implications of molecular composition and exosomal heterogeneity. J Control Release *228*, 179-190.

20. Friedenstein, A.J., Chailakhjan, R.K., and Lalykina, K.S. (1970). The development of fibroblast colonies in monolayer cultures of guinea-pig bone marrow and spleen cells. Cell Tissue Kinet *3*, 393-403.

21. Galipeau, J. (2013). The mesenchymal stromal cells dilemma--does a negative phase III trial of random donor mesenchymal stromal cells in steroid-resistant graft-versus-host disease represent a death knell or a bump in the road? Cytotherapy *15*, 2-8.

22. Garcia, J.H., Liu, K.F., Yoshida, Y., Lian, J., Chen, S., and del Zoppo, G.J. (1994). Influx of leukocytes and platelets in an evolving brain infarct (Wistar rat). Am J Pathol *144*, 188-199.

23. Gelderblom, M., Leypoldt, F., Steinbach, K., Behrens, D., Choe, C.U., Siler, D.A., Arumugam, T.V., Orthey, E., Gerloff, C., Tolosa, E., and Magnus, T. (2009). Temporal and spatial dynamics of cerebral immune cell accumulation in stroke. Stroke *40*, 1849-1857.

24. Gnecchi, M., Danieli, P., Malpasso, G., and Ciuffreda, M.C. (2016). Paracrine Mechanisms of Mesenchymal Stem Cells in Tissue Repair. Methods Mol Biol *1416*, 123-146.

25. Han, Y.D., Bai, Y., Yan, X.L., Ren, J., Zeng, Q., Li, X.D., Pei, X.T., and Han, Y. (2018). Co-transplantation of exosomes derived from hypoxia-preconditioned adipose mesenchymal stem cells promotes neovascularization and graft survival in fat grafting. Biochem Biophys Res Commun *497*, 305-312.

26. Hermann, D.M., and Gunzer, M. (2019). Polymorphonuclear Neutrophils Play a Decisive Role for Brain Injury and Neurological Recovery Poststroke. Stroke *50*, e40-e41.

27. Hermann, D.M., Kleinschnitz, C., and Gunzer, M. (2018). Role of polymorphonuclear neutrophils in the reperfused ischemic brain: insights from cell-type-specific immunodepletion and fluorescence microscopy studies. Ther Adv Neurol Disord *11*, 1756286418798607.

28. Herz, J., Sabellek, P., Lane, T.E., Gunzer, M., Hermann, D.M., and Doeppner, T.R. (2015). Role of Neutrophils in Exacerbation of Brain Injury After Focal Cerebral Ischemia in Hyperlipidemic Mice. Stroke *46*, 2916-2925.

29. Iadecola, C., and Anrather, J. (2011). The immunology of stroke: from mechanisms to translation. Nat Med *17*, 796-808.

30. Jickling, G.C., Liu, D., Ander, B.P., Stamova, B., Zhan, X., and Sharp, F.R. (2015). Targeting neutrophils in ischemic stroke: translational insights from experimental studies. J Cereb Blood Flow Metab *35*, 888-901.

31. Joel, M.D.M., Yuan, J., Wang, J., Yan, Y., Qian, H., Zhang, X., Xu, W., and Mao, F. (2019). MSC: immunoregulatory effects, roles on neutrophils and evolving clinical potentials. Am J Transl Res *11*, 3890-3904.

32. Kenne, E., Erlandsson, A., Lindbom, L., Hillered, L., and Clausen, F. (2012). Neutrophil depletion reduces edema formation and tissue loss following traumatic brain injury in mice. J Neuroinflammation *9*, 17.

33. Kim, S.Y., Khanal, D., Kalionis, B., and Chrzanowski, W. (2019). High-fidelity probing of the structure and heterogeneity of extracellular vesicles by resonance-enhanced atomic force microscopy infrared spectroscopy. Nat Protoc *14*, 576-593.

34. Klingemann, H., Matzilevich, D., and Marchand, J. (2008). Mesenchymal Stem Cells - Sources and Clinical Applications. Transfus Med Hemother *35*, 272-277.

35. Kopen, G.C., Prockop, D.J., and Phinney, D.G. (1999). Marrow stromal cells migrate throughout forebrain and cerebellum, and they differentiate into astrocytes after injection into neonatal mouse brains. Proc Natl Acad Sci U S A *96*, 10711-10716.

36. Kordelas, L., Rebmann, V., Ludwig, A.K., Radtke, S., Ruesing, J., Doeppner, T.R., Epple, M., Horn, P.A., Beelen, D.W., and Giebel, B. (2014). MSC-derived exosomes: a novel tool to treat therapy-refractory graft-versus-host disease. Leukemia *28*, 970-973.

37. Le Blanc, K., Frassoni, F., Ball, L., Locatelli, F., Roelofs, H., Lewis, I., Lanino, E., Sundberg, B., Bernardo, M.E., Remberger, M., Dini, G., Egeler, R.M., Bacigalupo, A., Fibbe, W., and Ringden, O. (2008). Mesenchymal stem cells for treatment of steroid-resistant, severe, acute graft-versus-host disease: a phase II study. Lancet *371*, 1579-1586.

38. Le Blanc, K., Rasmusson, I., Sundberg, B., Gotherstrom, C., Hassan, M., Uzunel, M., and Ringden, O. (2004). Treatment of severe acute graft-versus-host disease with third party haploidentical mesenchymal stem cells. Lancet *363*, 1439-1441.

39. Lener, T., Gimona, M., Aigner, L., Borger, V., Buzas, E., Camussi, G., Chaput, N., Chatterjee, D., Court, F.A., Del Portillo, H.A., ODriscoll, L., Fais, S., Falcon-Perez, J.M., Felderhoff-Mueser, U., Fraile, L., Gho, Y.S., Gorgens, A., Gupta, R.C., Hendrix, A., Hermann, D.M., Hill, A.F., Hochberg, F., Horn, P.A., de Kleijn, D., Kordelas, L., Kramer, B.W., Kramer-Albers, E.M., Laner-Plamberger, S., Laitinen, S., Leonardi, T., Lorenowicz, M.J., Lim, S.K., Lotvall, J., Maguire, C.A., Marcilla, A., Nazarenko, I., Ochiya, T., Patel, T., Pedersen, S., Pocsfalvi, G., Pluchino, S., Quesenberry, P., Reischl, I.G., Rivera, F.J., Sanzenbacher, R., Schallmoser, K., Slaper-Cortenbach, I., Strunk, D., Tonn, T., Vader, P., van Balkom, B.W., Wauben, M., Andaloussi, S.E., Thery, C., Rohde, E., and Giebel, B. (2015). Applying extracellular vesicles based therapeutics in clinical trials - an ISEV

position paper. J Extracell Vesicles *4*, 30087.

40. Levy, M.L., Crawford, J.R., Dib, N., Verkh, L., Tankovich, N., and Cramer, S.C. (2019). Phase I/II Study of Safety and Preliminary Efficacy of Intravenous Allogeneic Mesenchymal Stem Cells in Chronic Stroke. Stroke *50*, 2835-2841.

41. Li, Q.C., Liang, Y., and Su, Z.B. (2019). Prophylactic treatment with MSC-derived exosomes attenuates traumatic acute lung injury in rats. Am J Physiol Lung Cell Mol Physiol *316*, L1107-l1117.

42. Li, Y., Chen, J., Chen, X.G., Wang, L., Gautam, S.C., Xu, Y.X., Katakowski, M., Zhang, L.J., Lu, M., Janakiraman, N., and Chopp, M. (2002). Human marrow stromal cell therapy for stroke in rat: neurotrophins and functional recovery. Neurology *59*, 514-523.

43. Liu, W., Li, L., Rong, Y., Qian, D., Chen, J., Zhou, Z., Luo, Y., Jiang, D., Cheng, L., Zhao, S., Kong, F., Wang, J., Zhou, Z., Xu, T., Gong, F., Huang, Y., Gu, C., Zhao, X., Bai, J., Wang, F., Zhao, W., Zhang, L., Li, X., Yin, G., Fan, J., and Cai, W. (2019). Hypoxic mesenchymal stem cell-derived exosomes promote bone fracture healing by the transfer of miR-126. Acta Biomater. DOI: 10.1016/j.actbio.2019.12.020

44. Ludwig, A.K., De Miroschedji, K., Doeppner, T.R., Borger, V., Ruesing, J., Rebmann, V., Durst, S., Jansen, S., Bremer, M., Behrmann, E., Singer, B.B., Jastrow, H., Kuhlmann, J.D., El Magraoui, F., Meyer, H.E., Hermann, D.M., Opalka, B., Raunser, S., Epple, M., Horn, P.A., and Giebel, B. (2018). Precipitation with polyethylene glycol followed by washing and pelleting by ultracentrifugation enriches extracellular vesicles from tissue culture supernatants in small and large scales. J Extracell Vesicles *7*, 1528109.

45. Maestrini, I., Strbian, D., Gautier, S., Haapaniemi, E., Moulin, S., Sairanen, T., Dequatre-Ponchelle, N., Sibolt, G., Cordonnier, C., Melkas, S., Leys, D., Tatlisumak, T., and Bordet, R. (2015). Higher neutrophil counts before thrombolysis for cerebral ischemia predict worse outcomes. Neurology *85*, 1408-1416.

46. Martin, P.J., Uberti, J.P., Soiffer, R.J., Klingemann, H., Waller, E.K., Daly, A.S., Herrmann, R.P., and Kebriaei, P. (2010). Prochymal Improves Response Rates In Patients With Steroid-Refractory Acute Graft Versus Host Disease (SR-GVHD) Involving The

Liver And Gut: Results Of A Randomized, Placebo-Controlled, Multicenter Phase III Trial In GVHD. Biol Blood Marrow Transplant *16*, S169-S170.

47. Matsuo, Y., Onodera, H., Shiga, Y., Nakamura, M., Ninomiya, M., Kihara, T., and Kogure, K. (1994). Correlation between myeloperoxidase-quantified neutrophil accumulation and ischemic brain injury in the rat. Effects of neutrophil depletion. Stroke *25*, 1469-1475.

48. Mohd Ali, N., Boo, L., Yeap, S.K., Ky, H., Satharasinghe, D.A., Liew, W.C., Ong, H.K., Cheong, S.K., and Kamarul, T. (2016). Probable impact of age and hypoxia on proliferation and microRNA expression profile of bone marrow-derived human mesenchymal stem cells. PeerJ *4*, e1536.

49. National Institute of Neurological Disorders and Stroke rt-PA Stroke Study Group (1995). Tissue Plasminogen Activator for Acute Ischemic Stroke. N Engl J Med *333*, 1581-1588.

50. Neumann, J., Riek-Burchardt, M., Herz, J., Doeppner, T.R., Konig, R., Hutten, H., Etemire, E., Mann, L., Klingberg, A., Fischer, T., Gortler, M.W., Heinze, H.J., Reichardt, P., Schraven, B., Hermann, D.M., Reymann, K.G., and Gunzer, M. (2015). Very-late-antigen-4 (VLA-4)-mediated brain invasion by neutrophils leads to interactions with microglia, increased ischemic injury and impaired behavior in experimental stroke. Acta Neuropathol *129*, 259-277.

51. Peng, Y., Chen, X., Liu, Q., Zhang, X., Huang, K., Liu, L., Li, H., Zhou, M., Huang, F., Fan, Z., Sun, J., Liu, Q., Ke, M., Li, X., Zhang, Q., and Xiang, A.P. (2015). Mesenchymal stromal cells infusions improve refractory chronic graft versus host disease through an increase of CD5+ regulatory B cells producing interleukin 10. Leukemia *29*, 636-646.

52. Perets, N., Betzer, O., Shapira, R., Brenstein, S., Angel, A., Sadan, T., Ashery, U., Popovtzer, R., and Offen, D. (2019). Golden Exosomes Selectively Target Brain Pathologies in Neurodegenerative and Neurodevelopmental Disorders. Nano Letters *19*, 3422-3431.

53. Phinney, D.G. (2012). Functional heterogeneity of mesenchymal stem cells: Implications for cell therapy. J Cell Biochem *113*, 2806-2812.

54. Poirier, J., and Derouesné, C. (1993). Apoplexy and Stroke. In The Cambridge World History of Human Disease, K.F. Kiple, ed. (Cambridge: Cambridge University Press), pp. 584-587.

55. Radtke, S., Görgens, A., Liu, B., Horn, P.A., and Giebel, B. (2016). Human mesenchymal and murine stromal cells support human lympho-myeloid progenitor expansion but not maintenance of multipotent haematopoietic stem and progenitor cells. Cell Cycle *15*, 540-545.

56. Ringden, O., Uzunel, M., Rasmusson, I., Remberger, M., Sundberg, B., Lonnies, H., Marschall, H.U., Dlugosz, A., Szakos, A., Hassan, Z., Omazic, B., Aschan, J., Barkholt, L., and Le Blanc, K. (2006). Mesenchymal stem cells for treatment of therapy-resistant graft-versus-host disease. Transplantation *81*, 1390-1397.

57. Saad, A., Zhu, X.-Y., Herrmann, S., Hickson, L., Tang, H., Dietz, A.B., van Wijnen, A.J., Lerman, L., and Textor, S. (2016). Adipose-derived mesenchymal stem cells from patients with atherosclerotic renovascular disease have increased DNA damage and reduced angiogenesis that can be modified by hypoxia. Stem Cell Res Ther *7*, 128.

58. Sanchez-Ramos, J., Song, S., Cardozo-Pelaez, F., Hazzi, C., Stedeford, T., Willing, A., Freeman, T.B., Saporta, S., Janssen, W., Patel, N., Cooper, D.R., and Sanberg, P.R. (2000). Adult Bone Marrow Stromal Cells Differentiate into Neural Cells in Vitro. Exp Neurol *164*, 247-256.

59. Sansing, L.H., Harris, T.H., Kasner, S.E., Hunter, C.A., and Kariko, K. (2011). Neutrophil depletion diminishes monocyte infiltration and improves functional outcome after experimental intracerebral hemorrhage. Acta Neurochir Suppl *111*, 173-178.

60. Sarmah, D., Agrawal, V., Rane, P., Bhute, S., Watanabe, M., Kalia, K., Ghosh, Z., Dave, K.R., Yavagal, D.R., and Bhattacharya, P. (2018). Mesenchymal Stem Cell Therapy in Ischemic Stroke: A Meta-analysis of Preclinical Studies. Clin Pharmacol Ther *103*, 990-998.

61. Schafer, R., Spohn, G., and Baer, P.C. (2016). Mesenchymal Stem/Stromal Cells in Regenerative Medicine: Can Preconditioning Strategies Improve Therapeutic Efficacy? Transfus Med Hemother *43*, 256-267.

62. Shah, R., Patel, T., and Freedman, J.E. (2018). Circulating Extracellular Vesicles in Human Disease. N Engl J Med *379*, 958-966.

63. Shi, Y., Wang, Y., Li, Q., Liu, K., Hou, J., Shao, C., and Wang, Y. (2018). Immunoregulatory mechanisms of mesenchymal stem and stromal cells in inflammatory diseases. Nat Rev Nephrol *14*, 493-507.

64. Sokolova, V., Ludwig, A.K., Hornung, S., Rotan, O., Horn, P.A., Epple, M., and Giebel, B. (2011). Characterisation of exosomes derived from human cells by nanoparticle tracking analysis and scanning electron microscopy. Colloids Surf B Biointerfaces *87*, 146-150.

65. Taylor, T.N., Davis, P.H., Torner, J.C., Holmes, J., Meyer, J.W., and Jacobson, M.F. (1996). Lifetime Cost of Stroke in the United States. Stroke *27*, 1459-1466.

66. Théry, C., Witwer, K.W., Aikawa, E., Alcaraz, M.J., Anderson, J.D., Andriantsitohaina, R., Antoniou, A., Arab, T., Archer, F., Atkin-Smith, G.K., Ayre, D.C., Bach, J.-M., Bachurski, D., Baharvand, H., Balaj, L., Baldacchino, S., Bauer, N.N., Baxter, A.A., Bebawy, M., Beckham, C., Bedina Zavec, A., Benmoussa, A., Berardi, A.C., Bergese, P., Bielska, E., Blenkiron, C., Bobis-Wozowicz, S., Boilard, E., Boireau, W., Bongiovanni, A., Borràs, F.E., Bosch, S., Boulanger, C.M., Breakefield, X., Breglio, A.M., Brennan, M.Á., Brigstock, D.R., Brisson, A., Broekman, M.L.D., Bromberg, J.F., Bryl-Górecka, P., Buch, S., Buck, A.H., Burger, D., Busatto, S., Buschmann, D., Bussolati, B., Buzás, E.I., Byrd, J.B., Camussi, G., Carter, D.R.F., Caruso, S., Chamley, L.W., Chang, Y.-T., Chen, C., Chen, S., Cheng, L., Chin, A.R., Clayton, A., Clerici, S.P., Cocks, A., Cocucci, E., Coffey, R.J., Cordeiro-da-Silva, A., Couch, Y., Coumans, F.A.W., Coyle, B., Crescitelli, R., Criado, M.F., D'Souza-Schorey, C., Das, S., Datta Chaudhuri, A., de Candia, P., De Santana, E.F., De Wever, O., del Portillo, H.A., Demaret, T., Deville, S., Devitt, A., Dhondt, B., Di Vizio, D., Dieterich, L.C., Dolo, V., Dominguez Rubio, A.P.,

Dominici, M., Dourado, M.R., Driedonks, T.A.P., Duarte, F.V., Duncan, H.M., Eichenberger, R.M., Ekström, K., El Andaloussi, S., Elie-Caille, C., Erdbrügger, U., Falcón-Pérez, J.M., Fatima, F., Fish, J.E., Flores-Bellver, M., Försönits, A., Frelet-Barrand, A., Fricke, F., Fuhrmann, G., Gabrielsson, S., Gámez-Valero, A., Gardiner, C., Gärtner, K., Gaudin, R., Gho, Y.S., Giebel, B., Gilbert, C., Gimona, M., Giusti, I., Goberdhan, D.C.I., Görgens, A., Gorski, S.M., Greening, D.W., Gross, J.C., Gualerzi, A., Gupta, G.N., Gustafson, D., Handberg, A., Haraszti, R.A., Harrison, P., Hegyesi, H., Hendrix, A., Hill, A.F., Hochberg, F.H., Hoffmann, K.F., Holder, B., Holthofer, H., Hosseinkhani, B., Hu, G., Huang, Y., Huber, V., Hunt, S., Ibrahim, A.G.-E., Ikezu, T., Inal, J.M., Isin, M., Ivanova, A., Jackson, H.K., Jacobsen, S., Jay, S.M., Jayachandran, M., Jenster, G., Jiang, L., Johnson, S.M., Jones, J.C., Jong, A., Jovanovic-Talisman, T., Jung, S., Kalluri, R., Kano, S.-i., Kaur, S., Kawamura, Y., Keller, E.T., Khamari, D., Khomyakova, E., Khvorova, A., Kierulf, P., Kim, K.P., Kislinger, T., Klingeborn, M., Klinke, D.J., Kornek, M., Kosanović, M.M., Kovács, Á.F., Krämer-Albers, E.-M., Krasemann, S., Krause, M., Kurochkin, I.V., Kusuma, G.D., Kuypers, S., Laitinen, S., Langevin, S.M., Languino, L.R., Lannigan, J., Lässer, C., Laurent, L.C., Lavieu, G., Lázaro-Ibáñez, E., Le Lay, S., Lee, M.-S., Lee, Y.X.F., Lemos, D.S., Lenassi, M., Leszczynska, A., Li, I.T.S., Liao, K., Libregts, S.F., Ligeti, E., Lim, R., Lim, S.K., Linē, A., Linnemannstöns, K., Llorente, A., Lombard, C.A., Lorenowicz, M.J., Lörincz, Á.M., Lötvall, J., Lovett, J., Lowry, M.C., Loyer, X., Lu, Q., Lukomska, B., Lunavat, T.R., Maas, S.L.N., Malhi, H., Marcilla, A., Mariani, J., Mariscal, J., Martens-Uzunova, E.S., Martin-Jaular, L., Martinez, M.C., Martins, V.R., Mathieu, M., Mathivanan, S., Maugeri, M., McGinnis, L.K., McVey, M.J., Meckes, D.G., Meehan, K.L., Mertens, I., Minciacchi, V.R., Möller, A., Møller Jørgensen, M., Morales-Kastresana, A., Morhayim, J., Mullier, F., Muraca, M., Musante, L., Mussack, V., Muth, D.C., Myburgh, K.H., Najrana, T., Nawaz, M., Nazarenko, I., Nejsum, P., Neri, C., Neri, T., Nieuwland, R., Nimrichter, L., Nolan, J.P., Nolte-'t Hoen, E.N.M., Noren Hooten, N., O'Driscoll, L., O'Grady, T., O'Loghlen, A., Ochiya, T., Olivier, M., Ortiz, A., Ortiz, L.A., Osteikoetxea, X.,

Østergaard, O., Ostrowski, M., Park, J., Pegtel, D.M., Peinado, H., Perut, F., Pfaffl, M.W., Phinney, D.G., Pieters, B.C.H., Pink, R.C., Pisetsky, D.S., Pogge von Strandmann, E., Polakovicova, I., Poon, I.K.H., Powell, B.H., Prada, I., Pulliam, L., Quesenberry, P., Radeghieri, A., Raffai, R.L., Raimondo, S., Rak, J., Ramirez, M.I., Raposo, G., Rayyan, M.S., Regev-Rudzki, N., Ricklefs, F.L., Robbins, P.D., Roberts, D.D., Rodrigues, S.C., Rohde, E., Rome, S., Rouschop, K.M.A., Rughetti, A., Russell, A.E., Saá, P., Sahoo, S., Salas-Huenuleo, E., Sánchez, C., Saugstad, J.A., Saul, M.J., Schiffelers, R.M., Schneider, R., Schøyen, T.H., Scott, A., Shahaj, E., Sharma, S., Shatnyeva, O., Shekari, F., Shelke, G.V., Shetty, A.K., Shiba, K., Siljander, P.R.M., Silva, A.M., Skowronek, A., Snyder, O.L., Soares, R.P., Sódar, B.W., Soekmadji, C., Sotillo, J., Stahl, P.D., Stoorvogel, W., Stott, S.L., Strasser, E.F., Swift, S., Tahara, H., Tewari, M., Timms, K., Tiwari, S., Tixeira, R., Tkach, M., Toh, W.S., Tomasini, R., Torrecilhas, A.C., Tosar, J.P., Toxavidis, V., Urbanelli, L., Vader, P., van Balkom, B.W.M., van der Grein, S.G., Van Deun, J., van Herwijnen, M.J.C., Van Keuren-Jensen, K., van Niel, G., van Royen, M.E., van Wijnen, A.J., Vasconcelos, M.H., Vechetti, I.J., Veit, T.D., Vella, L.J., Velot, É., Verweij, F.J., Vestad, B., Viñas, J.L., Visnovitz, T., Vukman, K.V., Wahlgren, J., Watson, D.C., Wauben, M.H.M., Weaver, A., Webber, J.P., Weber, V., Wehman, A.M., Weiss, D.J., Welsh, J.A., Wendt, S., Wheelock, A.M., Wiener, Z., Witte, L., Wolfram, J., Xagorari, A., Xander, P., Xu, J., Yan, X., Yáñez-Mó, M., Yin, H., Yuana, Y., Zappulli, V., Zarubova, J., Žėkas, V., Zhang, J.-y., Zhao, Z., Zheng, L., Zheutlin, A.R., Zickler, A.M., Zimmermann, P., Zivkovic, A.M., Zocco, D., and Zuba-Surma, E.K. (2018). Minimal information for studies of extracellular vesicles 2018 (MISEV2018): a position statement of the International Society for Extracellular Vesicles and update of the MISEV2014 guidelines. J Extracell Vesicles *7*, 1535750.

67. Tkach, M., and Théry, C. (2016). Communication by Extracellular Vesicles: Where We Are and Where We Need to Go. Cell *164*, 1226-1232.

68. Vagner, T., Chin, A., Mariscal, J., Bannykh, S., Engman, D.M., and Di Vizio, D. (2019). Protein Composition Reflects Extracellular Vesicle Heterogeneity.

PROTEOMICS *19*, 1800167.

69. Veltkamp, R., and Gill, D. (2016). Clinical Trials of Immunomodulation in Ischemic Stroke. Neurotherapeutics *13*, 791-800.

70. Wardlaw, J.M., Murray, V., Berge, E., and del Zoppo, G.J. (2014). Thrombolysis for acute ischaemic stroke. Cochrane Database Syst Rev, Cd000213.

71. Willis, G.R., Kourembanas, S., and Mitsialis, S.A. (2017). Toward Exosome-Based Therapeutics: Isolation, Heterogeneity, and Fit-for-Purpose Potency. Front Cardiovasc Med *4*, 63.

72. Xin, H., Katakowski, M., Wang, F., Qian, J.Y., Liu, X.S., Ali, M.M., Buller, B., Zhang, Z.G., and Chopp, M. (2017a). MicroRNA cluster miR-17-92 Cluster in Exosomes Enhance Neuroplasticity and Functional Recovery After Stroke in Rats. Stroke *48*, 747-753.

73. Xin, H., Li, Y., Cui, Y., Yang, J.J., Zhang, Z.G., and Chopp, M. (2013a). Systemic administration of exosomes released from mesenchymal stromal cells promote functional recovery and neurovascular plasticity after stroke in rats. J Cereb Blood Flow Metab *33*, 1711-1715.

74. Xin, H., Li, Y., Liu, Z., Wang, X., Shang, X., Cui, Y., Zhang, Z.G., and Chopp, M. (2013b). MiR-133b promotes neural plasticity and functional recovery after treatment of stroke with multipotent mesenchymal stromal cells in rats via transfer of exosome-enriched extracellular particles. Stem Cells *31*, 2737-2746.

75. Xin, H., Wang, F., Li, Y., Lu, Q.-E., Cheung, W.L., Zhang, Y., Zhang, Z.G., and Chopp, M. (2017b). Secondary Release of Exosomes from Astrocytes Contributes to the Increase in Neural Plasticity and Improvement of Functional Recovery after Stroke in Rats Treated with Exosomes Harvested from MicroRNA 133b-Overexpressing Multipotent Mesenchymal Stromal Cells. Cell Transplant *26*, 243-257.

76. Xu, S.-Y., and Pan, S.-Y. (2013). The failure of animal models of neuroprotection in acute ischemic stroke to translate to clinical efficacy. Med Sci Monit Basic Res *19*, 37-45.

77. Xue, C., Shen, Y., Li, X., Li, B., Zhao, S., Gu, J., Chen, Y., Ma, B., Wei, J., Han, Q., and Zhao, R.C. (2018). Exosomes Derived from Hypoxia-Treated Human Adipose Mesenchymal Stem Cells Enhance Angiogenesis Through the PKA Signaling Pathway. Stem Cells Dev *27*, 456-465.

78. Xue, J., Huang, W., Chen, X., Li, Q., Cai, Z., Yu, T., and Shao, B. (2017). Neutrophil-to-Lymphocyte Ratio Is a Prognostic Marker in Acute Ischemic Stroke. J Stroke Cerebrovasc Dis *26*, 650-657.

79. Zhang, Z.G., Buller, B., and Chopp, M. (2019). Exosomes — beyond stem cells for restorative therapy in stroke and neurological injury. Nat Rev Neurol *15*, 193-203.

80. Zhu, J., Lu, K., Zhang, N., Zhao, Y., Ma, Q., Shen, J., Lin, Y., Xiang, P., Tang, Y., Hu, X., Chen, J., Zhu, W., Webster, K.A., Wang, J., and Yu, H. (2018a). Myocardial reparative functions of exosomes from mesenchymal stem cells are enhanced by hypoxia treatment of the cells via transferring microRNA-210 in an nSMase2-dependent way. Artif Cells Nanomed Biotechnol *46*, 1659-1670.

81. Zhu, L.P., Tian, T., Wang, J.Y., He, J.N., Chen, T., Pan, M., Xu, L., Zhang, H.X., Qiu, X.T., Li, C.C., Wang, K.K., Shen, H., Zhang, G.G., and Bai, Y.P. (2018b). Hypoxia-elicited mesenchymal stem cell-derived exosomes facilitates cardiac repair through miR-125b-mediated prevention of cell death in myocardial infarction. Theranostics *8*, 6163-6177.

82. Zhu, Y.G., Feng, X.M., Abbott, J., Fang, X.H., Hao, Q., Monsel, A., Qu, J.M., Matthay, M.A., and Lee, J.W. (2014). Human mesenchymal stem cell microvesicles for treatment of Escherichia coli endotoxin-induced acute lung injury in mice. Stem Cells *32*, 116-125.

8. ATTACHMENT

8.1. List of abbreviations

ACA	anterior cerebral artery
ANOVA	analysis of variance
BBB	blood-brain barrier
BCA	bicinchoninic acid
CCA	common carotid artery
CXCR2	C-X-C motif chemokine receptor 2
DAB	diaminobenzidine
DAMPs	danger-associated molecular patterns
DMEM	Dulbecco's modified Eagle medium
DTT	dithiothreitol
dpi	days post-ischemia
ECA	external carotid artery
EVs	extracellular vesicles
FACS	fluorescence-activated cell sorting
FDA	Food and Drug Administration
GvHD	graft-versus-host disease
HEPES	4-(2-hydroxyethyl)-1-piperazineethanesulfonic acid
HLA	human leukocytes antigen
hPL	human platelet lysate
ICA	internal carotid artery
ICAM-1	intercellular adhesion molecule-1
IgG	Immunoglobulin G
IQR	interquartile range
ISCT	International Society of Cell and Gene Therapy

LDF	laser Doppler flowmetry
LSD	least significant differences
LPS	lipopolysaccharides
Ly6G	lymphocyte antigen 6 locus G
MCA	middle cerebral artery
MCAO	middle cerebral artery occlusion
MSCs	mesenchymal stem/stromal cells
MSC-sEVs	mesenchymal stromal cell-derived small extracellular vesicles
MVBs	multivesicular bodies
NeuN	neuronal nuclear antigen
N_2O	nitrous oxide
NTA	nanoparticle tracking analysis
O_2	oxygen
PBS	phosphate-buffered saline
PBS-T	phosphate-buffered saline with Tween-20
PEG	polyethylene glycol
PFA	paraformaldehyde
PMNs	polymorphonuclear neutrophils
PPA	pterygopalatine artery
PRRs	pattern recognition receptors
PVDF	polyvinylidene fluoride
ROI	regions of interest
RPMI	Roswell Park Memorial Institute
rtPA	recombinant tissue plasminogen activator
s.c.	subcutaneously
SD	standard deviation
SDS-PAGE	sodium dodecyl sulfate-polyacrylamide gel electrophoresis
TBS	Tris-buffered saline

TBS-T	Tris-buffered saline with Tween-20
TEM	transmission electron microscopy
TLRs	Toll-like receptors
TUNEL	terminal deoxynucleotidyl transferase dUTP nick end labeling
VLA-4	very-late-antigen-4

8.2. List of tables

8.3. List of figures

8.4. Statement of permission

This thesis is written based on our manuscript, which is currently in press in the journal *Stroke*.

Data from our collaborators AG Giebel at the Institute for Transfusion Medicine in University Hospital Essen and AG Gunzer at the Institute of Experimental Immunology and Imaging in University Hospital Essen are presented here with their permission.

9. ACKNOWLEDGEMENTS

In this moment, I would like to express my gratitude:

Firstly, I thank my supervisor, Prof. Dirk Hermann, for accepting me as a member of NeuroScienceLab and guiding me throughout my doctoral study. The NeuroScienceLab is truly a wonderful academic "home" with labmates from diverse countries — Germany, Russia, Brazil, Colombia, Iran, Pakistan, and China. I enjoy scientific discussion and culture exchange with them and I thrive in this comfortable and pleasant working atmosphere.

Besides my supervisor, I would like to thank my collaborators AG Giebel at the Institute for Transfusion Medicine in University Hospital Essen and AG Gunzer at the Institute of Experimental Immunology and Imaging in University Hospital Essen. Particularly, I thank Prof. Bernd Giebel, Dr. Verena Börger, and their team for bringing me into the exciting research field of extracellular vesicles (EVs) and supporting me with their knowledge. In addition, I thank Prof. Giebel for kindly offering me the permission to present their data in my thesis, which makes my thesis intact and better.

My sincere thanks also go to my warm-hearted colleagues: Britta Kaltwasser, Kristina Wagner, Nina Hagemann, Egor Dzyubenko, Maryam Sardari, Tayana Silva de Carvalho, Daniel Manrique, Ayan Mohamud Yusuf, Maria Zafar, and Jonas Gregorius.

Last but not the least, I would like to thank my family in China for their understanding and support.

10. CURRICULUM VITAE

"The curriculum vitae is not included in the online version for data protection reasons."